nature metabolism

ARTICLES

https://doi.org/10.1038/s42255-020-0170-4

Check for updates

Arousal-induced cortical activity triggers lactate release from astrocytes

Marc Zuend[1,2], Aiman S. Saab[1,2,7], Matthias T. Wyss[1,2,7], Kim David Ferrari[1,2], Ladina Hösli[1,2], Zoe J. Looser[1,2], Jillian L. Stobart[1,2], Jordi Duran[3,4], Joan J. Guinovart[3,4,5], L. Felipe Barros[6] and Bruno Weber[1,2] ✉

It has been suggested that, in states of arousal, release of noradrenaline and β-adrenergic signalling affect long-term memory formation by stimulating astrocytic lactate production from glycogen. However, the temporal relationship between cortical activity and cellular lactate fluctuations upon changes in arousal remains to be fully established. Also, the role of β-adrenergic signalling and brain glycogen metabolism on neural lactate dynamics in vivo is still unknown. Here, we show that an arousal-induced increase in cortical activity triggers lactate release into the extracellular space, and this correlates with a fast and prominent lactate dip in astrocytes. The immediate drop in astrocytic lactate concentration and the parallel increase in extracellular lactate levels underline an activity-dependent lactate release from astrocytes. Moreover, when β-adrenergic signalling is blocked or the brain is depleted of glycogen, the arousal-evoked cellular lactate surges are significantly reduced. We provide in vivo evidence that cortical activation upon arousal triggers lactate release from astrocytes, a rise in intracellular lactate levels mediated by β-adrenergic signalling and the mobilization of lactate from glycogen stores.

The brain is almost exclusively fuelled by glucose oxidation[1]. Acute elevations in brain activity are met with a transient net increase in aerobic glycolysis and the production of lactate that is released into the extracellular space[2,3]. However, the primary cellular source of this activity-driven lactate release remains a matter of debate[4–7]. A long-standing hypothesis is that astrocytes increase their glycolysis in response to neuronal activity to cover neuronal ATP demand with lactate[5,8]. Many studies have expanded this metabolic-support model (see references in ref. [7]). Nevertheless, in vivo evidence of activity-evoked lactate release from astrocytes to neurons is still unavailable. Clearly, neurons are able to maintain their activity in vivo with a lactate supply[9], and an in vivo lactate gradient from astrocytes to neurons favours astrocytic shuttling of lactate to neurons[10]. However, recent data suggested that neurons increase their glycolytic activity upon stimulation and may also release lactate[11].

At a behavioural level, lactate mobilization from glycogen, primarily stored in astrocytes, has been shown to promote long-term memory formation[3,12–14]. In particular, emotionally driven memory formation induced by stress or arousal involves β-adrenergic signalling and lactate release from astrocytes[15,16]. During arousal, noradrenaline released from locus coeruleus projections strongly activates astrocytes[17] and could have diverse metabolic functions, including activation of glycogenolysis[18–20]. Apart from serving as an energy substrate, lactate also regulates neuronal excitability by modulating ATP-sensitive potassium (K_{ATP}) channels[21,22] or through direct action on membrane receptors[23,24]. Despite evidence that lactate has various functions including the regulation of wakefulness, brain plasticity and memory consolidation, the pathways and mechanisms that mediate astrocytic lactate release in vivo remain to be determined.

In this paper, we have addressed the way in which fast changes in cortical activity modulate lactate dynamics in astrocytes and neurons in awake behaving mice. We found that a startle response triggers a rapid lactate release from astrocytes, which is followed by increased lactate levels in neurons. The startle-evoked lactate surges were in part mediated by β-adrenergic signalling and derived from glycogen stores. Our results show that cortical astrocytes integrate local neurosensory input and brain-wide neuromodulatory signals to cover immediate ambient energy needs in vivo.

Results

Lactate dynamics in neurons and astrocytes in response to acute isoflurane exposure. We studied how state-dependent changes in cortical activity affect neuronal and astrocytic lactate levels in awake behaving mice. Mice were trained for head-restrained, awake two-photon imaging of genetically encoded sensors for lactate (called Laconic[25]) and calcium (GCaMP6s[26] and RCaMP 1.07 (ref. [27])) (Fig. 1a and Extended Data Fig. 1). Volatile anaesthetics, such as isoflurane, are known to induce changes in cortical activity[28–30]. We exposed mice to isoflurane for 20 min (1.5%) while monitoring lactate level changes in cortical neurons and astrocytes (Extended Data Fig. 2). Prolonged exposure to isoflurane caused a significant increase in intracellular lactate levels in both astrocytes and neurons, which remained elevated during the isoflurane period. Critically, at the onset of isoflurane exposure (within 10–20 s) we observed a significant and transient drop in lactate levels specifically in astrocytes but not in neurons (Extended Data Fig. 2b,c). After stopping isoflurane, lactate levels completely recovered to baseline levels within 20.2 ± 6.0 min and 17.7 ± 7.1 min in neurons and astrocytes, respectively.

[1]Institute of Pharmacology and Toxicology, University of Zurich, Zurich, Switzerland. [2]Neuroscience Center Zurich, University of Zurich and ETH Zurich, Zurich, Switzerland. [3]Institute for Research in Biomedicine, The Barcelona Institute of Science and Technology, Barcelona, Spain. [4]Centro de Investigación Biomédica en Red de Diabetes y Enfermedades Metabólicas Asociadas, Madrid, Spain. [5]Department of Biochemistry and Molecular Biomedicine, University of Barcelona, Barcelona, Spain. [6]Centro de Estudios Científicos, Valdivia, Chile. [7]These authors contributed equally: Aiman S. Saab, Matthias T. Wyss. ✉e-mail: bweber@pharma.uzh.ch

Isoflurane exposure causes an initial arousal response before induction of anaesthesia. The biphasic lactate response observed in astrocytes upon isoflurane exposure, consisting of an initial dip, followed by a rise in lactate concentration (Extended Data Fig. 2c), could be triggered by distinct phases of isoflurane-induced brain states[29]. Isoflurane and other general anaesthetics are known to cause an initial arousal before the anaesthetized state[30,31]. Hence, we investigated the way in which our isoflurane protocol affects overall brain activity (Extended Data Fig. 3) and cortical calcium dynamics in neurons and astrocytes (Extended Data Fig. 4).

First, we studied brain-activity patterns with electroencephalography (EEG) recordings (Extended Data Fig. 3a–d). Indeed, exposure to isoflurane-elicited changes in EEG patterns (Extended Data Fig. 3a,b). We observed, within seconds of isoflurane exposure, a significant increase in high-frequency spectrum typically associated with cortical desynchronization[32,33]. Cortical desynchronization was followed by an increase in slow-wave oscillations until EEG patterns reached the burst suppression found during deep anaesthesia[34,35]. The initial EEG band shifts observed upon isoflurane exposure (Extended Data Fig. 3c,d) strongly correlated with changes normally observed during an arousal response[32,36]. This was further corroborated with electromyography (EMG) recordings and by monitoring the pupil response (Extended Data Fig. 3e,f). Acute pupil dilations are a noninvasive estimate of changes in brain states and neuromodulatory inputs to the cortex. In accordance with our EEG recordings, shortly after isoflurane exposure, EMG electrical activity significantly increased by 67.6 ± 21.5%, and pupils dilated by 51.3 ± 31.7% (Extended Data Fig. 3g,i). In the subsequent anaesthetized state, muscle activity (EMG) and pupil size were strongly reduced by 40.1 ± 16.5% and 47.0 ± 17.1%, respectively (Extended Data Fig. 3g,i). Taken together, our EEG, EMG and pupil-size measurements confirmed a rapid and transient arousal response before the onset of the anaesthetized state.

The state of elevated arousal has been shown to evoke cortical calcium bursts in astrocytes[17] and neurons[36]. We therefore examined cortical calcium activity during prolonged isoflurane exposure by monitoring cellular calcium dynamics using a combination of two calcium sensors, RCaMP 1.07 (ref. [27]) in neurons and GCaMP6s[26] in astrocytes, expressed in the same field of view (Extended Data Fig. 4). Immediately upon isoflurane exposure, there was a significant and transient elevation of calcium whole-frame fluorescence intensity in both neurons and astrocytes (Extended Data Fig. 4b,c). Moreover, automated analysis of calcium signals[37,38] revealed a twofold increase in calcium events in response to isoflurane exposure in both neurons and astrocytes (Extended Data Fig. 4d,e). Notably, during the subsequent anaesthetized state, calcium signal intensity and spontaneous activity in neurons and astrocytes were substantially reduced (Extended Data Fig. 4b–e). Both calcium fluorescence intensities and event frequencies returned to baseline values when isoflurane application was stopped. We found that the overall calcium dynamics observed in astrocytes and neurons are in line with our EEG, EMG and pupillometry measurements showing an initial increase in cellular activity upon isoflurane administration.

Arousal triggers lactate release from astrocytes. Our EEG, EMG and pupil-size measurements, as well as our cortical calcium recordings, provide convincing evidence that when administered, isoflurane initially causes an immediate, strong arousal response. Thus, we wondered whether brief isoflurane pulses would lead to arousal-evoked cortical lactate fluctuations. We therefore adapted our protocol and exposed awake mice to a brief 20-s isoflurane pulse (ISO pulse; Fig. 1b). As expected, the ISO pulse triggered a large pupil dilation without causing subsequent pupil constriction, indicating that we were only inducing a startle response (Fig. 1c,d). This was further corroborated by measuring cortical calcium dynamics. Indeed, the ISO pulse elicited a significant calcium transient in both neurons and astrocytes (Fig. 1e,f).

Next, we examined how arousal impacts lactate levels in cortical neurons and astrocytes. Arousal-induced calcium and lactate recordings were each performed in the same animal by using a multiviral injection approach (Extended Data Fig. 1d,e). In both neurons and astrocytes, lactate levels were significantly increased by 2.4 ± 1.3% and 3.6 ± 1.4%, respectively, in response to the ISO pulse (Fig. 1g,h). Strikingly, only astrocytes revealed a prominent lactate dip, by 2.1 ± 1.4%, before the subsequent lactate surge (Fig. 1h).

We then compared the time course of the evoked changes in EMG, pupil radius, calcium and lactate response in the arousal paradigm, and revealed the relationship between the initial dip and cortical states (Fig. 1i,j and Supplementary Fig. 1). In neurons, the evoked lactate surge appeared after the induced pupil dilation and calcium transients (Fig. 1i). In contrast, changes in cortical astrocytic lactate levels, calcium response and pupil radius occurred almost simultaneously (Fig. 1j). The minimum of the astrocytic lactate dip coincided with the peak of the astrocytic calcium response (lactate dip, 0.26 ± 0.14 min; calcium peak, 0.18 ± 0.08 min; $P = 0.24$; Fig. 1j). To further compare response kinetics between neurons and astrocytes, we computed the response slopes (Fig. 1k) of the lactate elevations. Notably, despite the initial lactate dip, astrocytes displayed a significantly faster lactate rise than that in neurons (Fig. 1i–k). These time courses highlight the rapid initiation of the astrocytic dip that correlates strongly with the onsets of pupil, EMG and neuronal calcium responses (Supplementary Fig. 1), suggesting a role for arousal.

To test for a role of a general increase in arousal in triggering the cellular lactate responses, we compared the ISO pulse protocol with other stimulation paradigms, such as single-whisker stimulation, a puff of air to the whisker pad, a short pulse of air and amyl acetate (Extended Data Fig. 5a–f), and varied the dose (Extended Data Fig. 5g–l) and time of the ISO pulse (Extended Data Fig. 5m–r). The 20-s ISO pulse elicited the strongest pupil response (Extended Data Fig. 5b,n) and cellular activation (Extended Data Fig. 5h), which resulted in nearly 60% of 104 imaged astrocytes showing a lactate

Fig. 1 | Startle-induced calcium and lactate elevation in neurons and astrocytes. a, Animals were trained to undergo head-restrained, awake, two-photon imaging. A water spout was used for reward delivery, and a ventilation mask for isoflurane supply. **b**, Paradigm followed to induce arousal in awake mice. **c**,**d**, A brief isoflurane pulse (ISO) induced pupil dilation (T5.2) without a subsequent miosis. White circles indicate pupil size approximation (**c**) used to calculate percentage changes from baseline values at T2 (**d**). **e**,**f**, Neurons (**e**) and astrocytes (**f**) immediately responded with an increase in calcium (T5.2) upon ISO pulse. Relative calcium changes normalized to baseline were quantified at time points T2, T5.2, T7 and T20 (bar graphs). The time point of isoflurane onset (T5) is indicated by ISO. **g**,**h**, Lactate level changes in neurons (**g**) and astrocytes (**h**). Arousal induced lactate level elevations in both cell types (T7). Note that only astrocytes revealed a significant dip in lactate levels immediately after the ISO pulse (T5.2). Quantification of relative lactate level changes at time points T2, T5.2, T7 and T20 (bar graphs). The dataset comprised 226 neurons and 236 astrocytes. **i**,**j**, Overlay of pupil (blue), calcium (black) and lactate responses (red) in neurons (**i**) and astrocytes (**j**). Note that in astrocytes the evoked calcium response strongly coincided with the immediate, initial drop in lactate levels. Dashed lines are indicated for slope analysis shown in **k**. **k**, Response slopes of the evoked lactate rise. Astrocytes had a faster lactate level rise (8.3 ± 1.1% per min) than did neurons (4.7 ± 3.3% per min; $P < 0.02$). T, time points in minutes; *N*, number of animals; *n*, number of experiments; *m*, size of dataset used for statistical analysis. Data are represented as mean ± s.d. $m = 8$ experiments for pupil, 12 for calcium and 12 for lactate used to derive statistics. Mean statistics were calculated using two-sided linear mixed-effects models and Tukey's post hoc tests.

dip (Extended Data Fig. 5e), whereas all astrocytes and nearly all neurons (120 cells) showed a lactate surge (Extended Data Fig. 5e). In addition, quantification of the percentage of responsive cells (that is, cells showing a stimulus-evoked lactate dip and/or surge larger than two times the s.d. from baseline values) revealed that the numbers of lactate-responding astrocytes and neurons strongly increased (Extended Data Fig. 5e,f,k,l,q,r) when the evoked relative pupil dilation and calcium response were larger (Extended

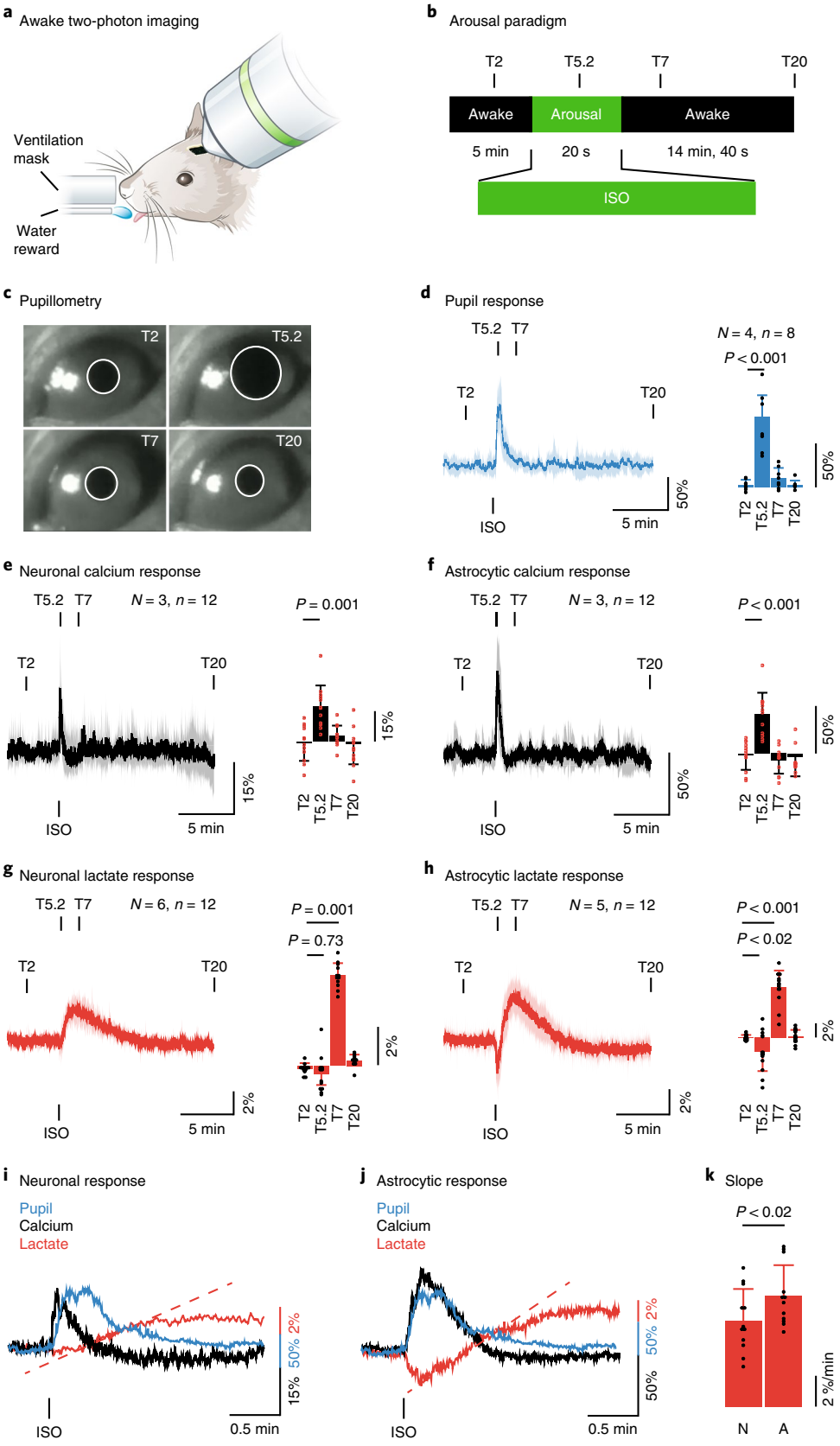

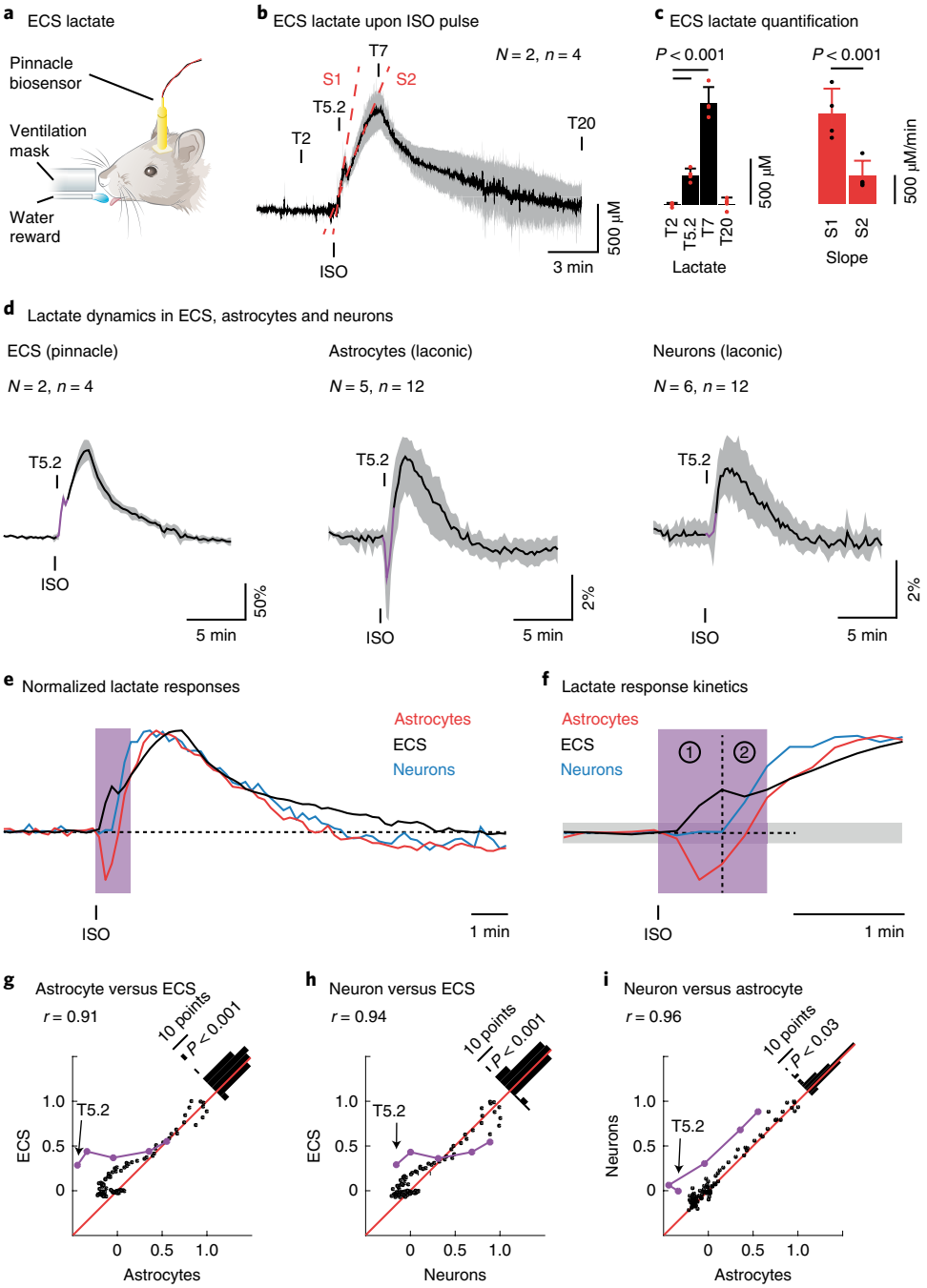

Fig. 2 | Lactate-response kinetics suggest an activity-dependent release of lactate from astrocytes. a, Scheme of ECS lactate recordings using a precalibrated Pinnacle lactate biosensor inserted into the somatosensory cortex. **b**, ECS lactate levels changed in response to ISO pulse. Note that the ECS lactate surge has two distinct slopes (S1 and S2; $P < 0.001$), indicated by dashed red lines. **c**, Quantification of ECS lactate surges. $m = 4$ experiments used to derive statistics. Mean statistics were calculated using two-tailed linear mixed-effects models and Tukey's post hoc tests at different time points. **d**, Direct comparison of the arousal-evoked lactate responses of the three compartments. Purple section of curves indicates the first 60 s upon ISO pulse. Data are represented as mean ± s.d. **e**, Normalized lactate responses from astrocytes, neurons and ECS. **f**, Magnification of the time course depicted in **e** around the ISO pulse to better visualize lactate response kinetics. The purple shaded area indicates the first 60 s upon ISO pulse, and the grey shaded area indicates margins of two s.d. from the baseline of all three recordings. Two distinct phases are highlighted. First phase (1): lactate level drop in astrocytes paralleled the rise in the ECS. Second phase (2): neuronal lactate rise slowed down the lactate surge in the ECS. **g**–**i**, Time series comparison of normalized data from **d** between neuronal, astrocytic and ECS responses. Direct comparison of ECS with astrocytes upon arousal (T5.2 onwards) showed a decrease in association and a significant left shift from the identity line (red), in favour of ECS lactate increases, as revealed by the distribution of data points in the histogram (top right corner). The overall comparison revealed that ECS showed the fastest increase in lactate levels followed by astrocytes and neurons. The arrow indicates the first data point after the ISO pulse (T5.2). $m = 12$ for neurons, $m = 12$ for astrocytes and $m = 4$ experiments used to derive statistics. Correlation (r) was computed with Pearson's linear correlation coefficient at a significance level of 0.05. Histogram (top right) shows the data distribution of mean values compared to identity line (correlation of 1; red) and statistical analysis of differences between compartments (two-tailed paired t-test).

Data Fig. 5b,h,n). Like the ISO pulse, the other stimuli triggered a pupil response (indicative of an increase in arousal; Extended Data Fig. 5b). They also induced cortical lactate fluctuations in both astrocytes and neurons (Extended Data Fig. 5c,d), confirming that our portrayed arousal-mediated lactate dynamics are not isoflurane specific. However, compared with the other stimulus paradigms, the ISO pulse was the strongest arousal-inducing paradigm. Astrocytic lactate dips and surges became larger and more frequent than with weaker stimulations. Thus, the ISO pulse seems to be an effective and robust paradigm for studying arousal-mediated global cortical lactate dynamics in awake mice.

The immediate arousal-mediated decrease in astrocytic lactate suggests an activity-dependent lactate consumption or release. If the latter were the case, we would expect to detect an arousal-evoked lactate release from astrocytes with a concomitant increase in extracellular lactate levels. We therefore measured changes in extracellular space (ECS) lactate levels, using a precalibrated lactate biosensor inserted into the somatosensory cortex (Fig. 2a). A brief isoflurane pulse caused a significant extracellular lactate rise of 1.10 ± 0.15 mM (Fig. 2b,c). Two distinct slopes were seen in these ECS lactate elevations. There was an initial, rapid lactate rise (S1, 25.8 ± 6.3 µM per s) that peaked around 35 s post stimulus, which was followed by a second, significantly slower component (S2, 8.1 ± 3.8 µM per s; Fig. 2b,c). We went on to compare the kinetics of lactate dynamics in the ECS, astrocytes and neurons (Fig. 2d–f). Two distinct phases in lactate dynamics were identifiable during the first 60 s: (1) a fast initial ECS lactate rise that coincided with the lactate decrease in astrocytes and (2) a slow delayed ECS lactate rise that coincided with the neuronal lactate increase (Fig. 2f). The differences in lactate dynamics between the three compartments were further corroborated by direct comparison of the time series of lactate level changes and kinetics within the initial 60 s of the arousal response (Fig. 2g–i). Hence, our data imply that astrocytes rapidly release lactate in an activity-dependent manner upon arousal.

β-adrenergic signalling mediates arousal-induced lactate-level surges. Changes in arousal are linked to the release of the neuromodulator noradrenaline in cortex, from neuronal locus coeruleus projections. In astrocytes, β-adrenergic signalling has been reported to shape emotionally driven memory formation[15], and β-signalling-mediated lactate shuttling from astrocytes to neurons plays a key role in associative learning[3,12,39]. Our experiments show that arousal impacts cortical lactate dynamics and that astrocytes are likely to release lactate upon cortical activation (Figs. 1 and 2). To assess whether noradrenergic inputs mediate the arousal-evoked cortical lactate mobilization, we tested the nonselective β-adrenergic receptor blocker propranolol in the arousal paradigm. Arousal-evoked lactate and calcium responses (Fig. 3 and Extended Data Fig. 6) in astrocytes and neurons were recorded before (0 h) and at several time points (1, 3, 6 and 24 h) after administration of propranolol (10 mg per kg (body weight), i.p.). With accurate, repetitive imaging, we followed arousal-evoked responses in the same cells over time (Supplementary Fig. 2). Blocking β-adrenergic receptors with propranolol did not impair evoked calcium transients in neurons or astrocytes (Extended Data Fig. 6b–f), a finding in line with those from previous reports[17]. In contrast, propranolol had a significant impact on the induced lactate surges in both neurons and astrocytes (Fig. 3b,c,e,f and Extended Data Fig. 6g,i), but caused no overt changes in the astrocytic lactate dip (Fig. 3d and Extended Data Fig. 6g,i). Lactate surges (Fig. 3e), response slopes (Fig. 3f), the percentage of responding cells with a surge (Extended Data Fig. 6h) and surge size of responding cells (Extended Data Fig. 6i) started to decrease compared with baseline responses within the first hour after drug injection. Twenty-four hours after injection of propranolol, lactate responses recovered completely. Control experiments with saline injections did not show any changes in the arousal-evoked calcium and lactate responses (Extended Data Fig. 7). These results suggest that β-adrenergic signalling appears to primarily regulate de novo lactate production and lactate mobilization from glucose or glycogen stores rather than acting directly on the astrocytic lactate-release machinery.

Brain glycogen fuels lactate responses in astrocytes and neurons. The arousal-evoked increase in cerebral activity induced cellular lactate fluctuations that partly derived from β-adrenergic signalling (Fig. 3). We wondered whether β-adrenergic signalling might regulate lactate mobilization from glycogen stores, as it has been proposed to occur in cultured astrocytes[20,40]. To test this possibility, we studied cortical metabolite dynamics and cellular activity in mice lacking brain glycogen[14] using glycogen synthase 1 (GYS1)-knockout mice ($Gys1^{flox/flox} \times$ Nestin-Cre = GYS1 KO; Fig. 4 and Extended Data Fig. 8). However, before studying cortical-activity-evoked lactate dynamics in GYS1 KO mice, we first questioned whether absence of brain glycogen by itself may have altered plasma metabolite levels, cellular activity and intracellular lactate levels, which may indirectly hamper the arousal-evoked cortical lactate dynamics. However, blood plasma glucose and lactate levels (Extended Data Fig. 8c) as well as cellular activity (Extended Data Fig. 8d) showed no difference between mutant and control mice. To asses possible changes in steady-state intracellular lactate levels, we first established the previously described pyruvate trans-acceleration protocol[10] in awake wild-type mice (Extended Data Fig. 9). Indeed, the trans-acceleration protocol with a systemic pyruvate injection confirmed that astrocytes have higher lactate levels than neurons[10] also in awake mice (Extended Data Fig. 9b,c). Moreover, with this one-point calibration protocol, we determined that intracellular lactate levels are not overtly changed in GYS1 KO mice compared with littermate controls (Extended Data Fig. 8e,f).

Next, we studied arousal-evoked cortical calcium and lactate dynamics in the absence of brain glycogen by using the ISO pulse paradigm. The evoked calcium responses of astrocytes and neurons in GYS1 mutants and littermate controls were similar in amplitude (Fig. 4a,b). However, the arousal-evoked lactate surges were significantly reduced in both astrocytes and neurons in GYS1 KO mice compared with controls (Fig. 4c,d). Notably, both GYS1 KO and controls had a similar number of lactate-responsive astrocytes and neurons to the ISO pulse, emphasizing that the decreased lactate surges in GYS1 KO mice are mainly due to impaired intracellular lactate mobilization (Extended Data Fig. 10a,b). The lactate dip in astrocytes was not significantly altered in GYS1 KO mice (Fig. 4d and Extended Data Fig. 10b). Overall, the changes in lactate fluctuations observed in GYS1 KO mice resembled the data when the β-adrenergic receptors were inhibited. Moreover, and in agreement with previous findings[3,12,41], GYS1-deficient mice exhibited impairments in associative learning (Extended Data Fig. 10c,d).

In summary, β-adrenergic signalling appears to primarily regulate lactate production and mobilization from glycogen stores rather than acting directly on the astrocytic lactate release machinery that is most likely directly regulated by cellular depolarization (Fig. 5). Additionally, these findings suggest that arousal-induced glycogen breakdown is critical to mobilize lactate that is required for higher cognitive functions.

Discussion

Acute brain activation is accompanied by an increase in aerobic glycolysis and surges in extracellular lactate. Our work here shows that arousal caused a fast and transient decrease in astrocytic lactate, and a corresponding increase in extracellular lactate followed by an increase in lactate in neurons and astrocytes (Figs. 1 and 2). Neuronal activity was increased at the same time (Fig. 1). We show that neither inhibition of β-adrenergic signalling with propranolol

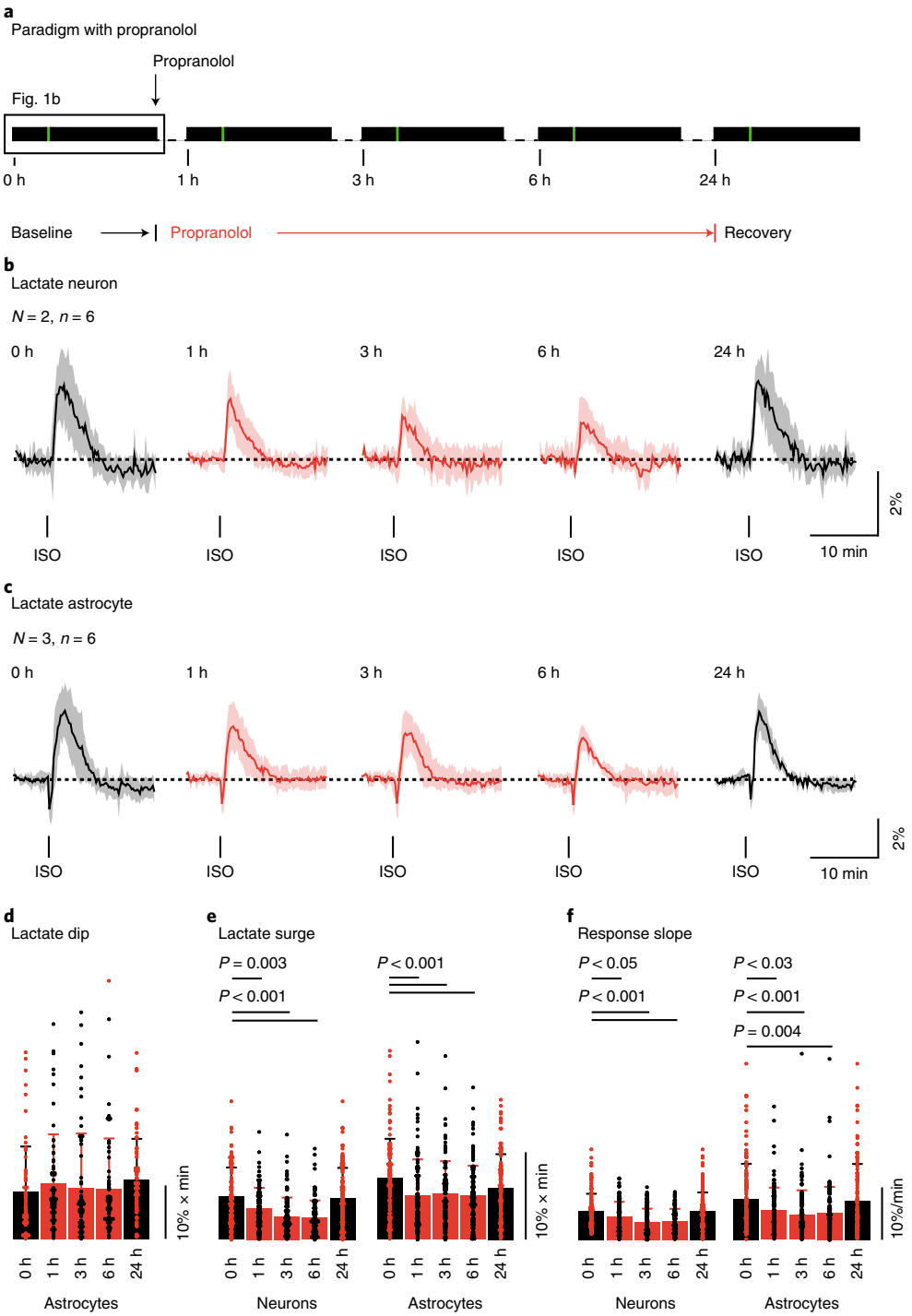

Fig. 3 | β-adrenergic signalling mediates startle-evoked lactate surges. a, Schematic of the investigation into the effects of propranolol (β-adrenergic antagonist) on arousal-induced lactate responses. Propranolol (10 mg per kg (body weight), i.p.) was injected after baseline acquisition (0 h). **b**,**c**, Evoked lactate responses in neurons (**b**) and astrocytes (**c**) before (0 h) and after propranolol injection (1, 3, 6 and 24 h). The same 113 neurons and 118 astrocytes were monitored per time point. **d**, Quantification of the area under the curve (AUC) of the evoked lactate dip in astrocytes before (0 h) and after propranolol (1–24 h) showed no change in the dip response. **e**,**f**, Quantification of startle-induced lactate surges (**e**) and response slopes (**f**) in neurons (left) and astrocytes (right) gradually decreased after propranolol injection (1–6 h) and recovered 24 h later. At 6 h after propranolol injection, arousal-evoked lactate surges, measured with the AUC, were reduced by 49.4 ± 40.2% and 31.2 ± 32.5% (both $P < 0.001$; Tukey's post hoc test). We also saw that the response slopes decreased by 35.3 ± 28.6% and 34.7 ± 25.3% compared with baseline responses in neurons and astrocytes, respectively ($P < 0.001$ and $P = 0.004$). *N*, number of animals; *n*, number of experiments. Data are represented as mean ± s.d. $m = 113$ neurons and 118 astrocytes used to derive statistics. Mean statistics were calculated using two-tailed linear mixed-effects models and Tukey's post hoc tests.

(Fig. 3) nor depletion of glycogen stores (Fig. 4) affected the initial astrocytic lactate release, but both were critical in controlling neuronal and astrocytic lactate surges.

We have introduced a startle paradigm to elicit a robust and reproducible arousal response in awake mice and combined it with two-photon microscopy used for high spatiotemporal imaging.

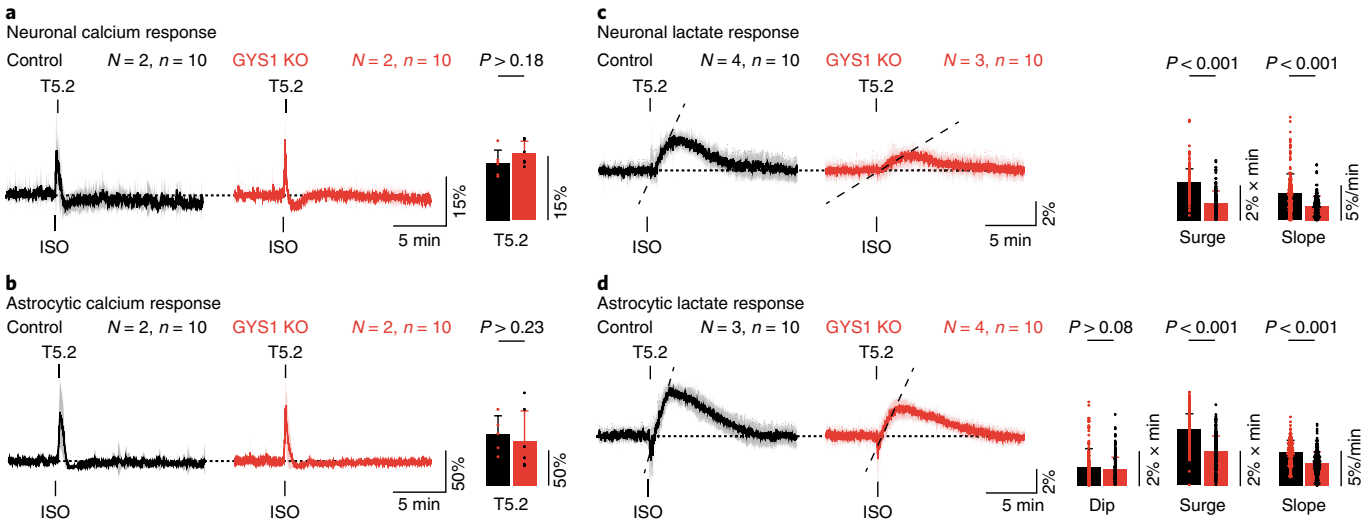

Fig. 4 | A lack of brain glycogen leads to impaired lactate responses in cortical neurons and astrocytes. a,**b**, Isoflurane-pulse-evoked calcium changes in neurons (**a**) and astrocytes (**b**) in control animals (black) and GYS1 KO mice (red). Calcium response in control and GYS1 KO mice did not differ (bar graph). **c**,**d**, Lactate-level fluctuations in control and GYS1 KO mice in neurons (**c**) and astrocytes (**d**). Bar graphs illustrate quantification of the AUC and slope responses. The dip was not affected when glycogen was lacking, but lactate increases were less pronounced in GYS1 KO mice (neurons, 3.4 ± 2.0% versus 5.0 ± 2.5% × min, $P < 0.001$; astrocytes, 4.6 ± 2.3% versus 6.6 ± 2.4% × min, $P < 0.001$) and raised slower (neurons: 2.0 ± 1.4% versus 3.8 ± 2.7% × min, $P < 0.001$; astrocytes, 3.1 ± 1.6% versus 4.7 ± 1.7% per min, $P < 0.001$). Dataset for control animals comprised 177 neurons and 146 astrocytes. Dataset for GYS1 KO animals comprised 184 neurons and 192 astrocytes. Dashed lines are indicated for slope analysis. T, time points in minutes. *N*, number of animals; *n*, number of experiments. Data are represented as mean ± s.d. *m* = 184 neurons and 192 astrocytes used to derive statistics. Mean statistics were calculated using two-tailed linear mixed-effects models and Tukey's post hoc tests.

Acute exposure to isoflurane induced a rapid arousal response[29,30], which we identified carefully by measuring EEG, EMG, pupil size and cortical calcium responses. Pupil dilation occurred within seconds of an isoflurane stimulus. Tracking pupil-diameter changes is a consistent method for monitoring wakefulness, switching between cortical states and arousal[36]. Our EEG recordings during the initial seconds of isoflurane exposure are also in line with EEG profiles obtained from cortical responses to locus coeruleus stimulation[42,43]. The activity of locus coeruleus projections is critical in the regulation of wakefulness and in promoting arousal[44,45]. Arousal induced by forced locomotion or by air puffs has been shown to evoke calcium transients in cortical astrocytes[17,46–48] and in neurons[36]. In a similar manner, our isoflurane-induced-arousal protocol triggered a robust calcium response in both astrocytes and neurons. Important to note is that by limiting isoflurane exposure to a brief 20-s pulse (Fig. 1), we produced only arousal, while avoiding the subsequent sedative state that appeared after prolonged isoflurane administration. This is substantiated by EEG, EMG, pupillometry and cellular-calcium measurements that clearly allow for differentiation between the arousal response and the anaesthetized state (Extended Data Figs. 3 and 4). Moreover, directly upon isoflurane administration, animals stopped performing the licking behaviour of the suppression-response task (Extended Data Fig. 3h,i), which is in line with the initial induction of arousal, as it has been recently described to occur with acute locus coeruleus activation[49].

To gain more mechanistic insight into how the lactate dip is possibly regulated in vivo, we showed that with increasing arousal-evoked cortical activity astrocytic lactate dips and surges were larger and more frequent (Extended Data Fig. 5). We compared single-whisker stimulation (90 Hz, 8 s), air puffs on the whisker pad (5 Hz, 3 s), air flow for 20 s and the odorant amyl acetate (1:1,000) for 20 s (ref. [50]) to our short-pulse ISO paradigm (Extended Data Fig. 5a–f). Like the ISO pulse, the other stimuli triggered a pupil response indicative of an increase in arousal. They also induced cortical lactate fluctuations in both astrocytes and neurons, confirming that our portrayed arousal-mediated lactate dynamics are not isoflurane specific. However, the signal changes were markedly smaller when compared with the ISO pulse (Extended Data Fig. 5c,d). In addition, regarding the number of responsive cells showing a dip and/or surge, the ISO pulse protocol showed the highest number of responsive cells (Extended Data Fig. 5e). Also, lower doses (Extended Data Fig. 5g–l) and shorter administration time (Extended Data Fig. 5m–r) reduced the arousal response, lactate mobilization and the number of responsive cells. On a more general note, since isoflurane is commonly used as an anaesthetic in neurophysiology, the initial effect of arousal should be considered when interpreting the data.

In summary, all paradigms elicited a lactate response, but only the ISO pulse evoked a strong, robust and reproducible global cortical activation. We showed that the arousal-induced lactate response in astrocytes and neurons was independent of isoflurane. We successfully established the isoflurane-pulse paradigm to reliably evoke arousal and global cortical activation that can be easily combined with behavioural training (water licking performance) during awake two-photon imaging.

We used genetically encoded sensors for calcium[26,27] and lactate[25] in cortical astrocytes and neurons to examine intracellular calcium and lactate dynamics in response to isoflurane-induced arousal (Fig. 1). Moreover, with a precalibrated Pinnacle lactate biosensor[10] inserted into the cortex, we also studied arousal-evoked lactate fluctuations in the ECS (Fig. 2). While monitoring lactate dynamics with high temporal resolution, we detected a rapid and significant lactate level decrease only in astrocytes upon arousal. The astrocytic lactate dip occurred almost simultaneously with the arousal-evoked calcium transients in neurons and astrocytes (Fig. 1). In principle, this dip in astrocytic lactate could either be due to an increase in lactate consumption (conversion to pyruvate) or to an increased release of lactate. If the latter, then we would expect a corresponding, rapid increase in ECS lactate levels. Indeed, arousal-evoked ECS lactate dynamics revealed two distinct lactate response slopes. Strikingly,

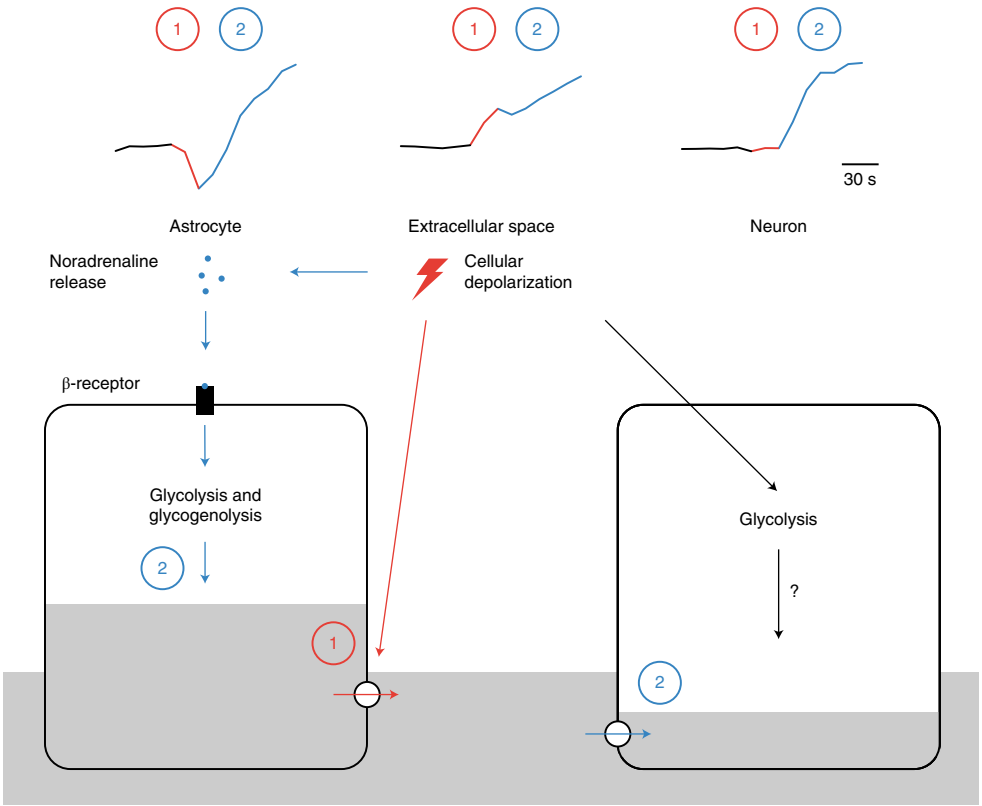

Fig. 5 | Model of startle-induced lactate mobilization from astrocytes. Arousal-induced cortical activity triggers an immediate lactate release from the astrocytic 'pressure reservoir'[56]. The grey shaded area represents steady-state lactate levels in all three compartments and highlights the lactate gradient from astrocytes to neurons[10]. The activity-evoked drop in astrocytic lactate is paralleled by a rapid rise in extracellular lactate levels (1, red). This initial astrocytic lactate release is most likely driven by cellular depolarization and a rise in extracellular $[K^+]$[51]. Moreover, arousal induces release of noradrenaline (NA) that activates β-adrenergic receptors on astrocytes. β-adrenergic signalling stimulates glycogenolysis in astrocytes[75], thereby promoting additional lactate production and release (2, blue). Neurons increase their lactate levels most likely by uptake of lactate, thereby slowing down the astrocyte-mediated extracellular lactate surge (2). Neurons may already take up lactate in the initial phase (1) which may be directly used to fuel cellular activity (arousal-evoked calcium transients; Fig. 2), resulting in balanced uptake and consumption. Neuronal depolarization may also stimulate glycolysis in neurons, which could contribute to the neuronal lactate rise[11].

we observed an initial, fast increase in ECS lactate of about 26 µM per s that coincided with the astrocytic lactate dip, suggesting that the rapid extracellular lactate rise is promoted by lactate release from astrocytes (Fig. 2). A very similar fast lactate release from astrocytes has been reported in response to acute extracellular $[K^+]$ elevations in vitro, to electrical stimulation in vivo and in hippocampal slices[51,52]. Hence, a rise in extracellular $[K^+]$ during neuronal activity could rapidly stimulate neighbouring astrocytes to release lactate, through a lactate channel[51], monocarboxylate transporters[53], or possibly via pannexins or hemichannels[54]. The initial decrease in astrocytic lactate was much steeper when animals were startled than with intracellular lactate depletion by trans-acceleration with pyruvate (Extended Data Fig. 9g,h). This result might indicate that cellular depolarization mediates a fast-channel-mediated lactate export, whereas trans-acceleration acts mainly on carrier-mediated intracellular lactate depletion through monocarboxylate transporters as described by others[10]. The overshoot in the ISO paradigm may have resulted from de novo lactate synthesis, whereas pyruvate conversion by lactate dehydrogenase led to increased lactate levels in neurons and astrocytes. Interestingly, with electrical stimulation in vitro, a dip was mainly observed without a subsequent increase in intracellular lactate[51,52], suggesting that a dip is not a prerequisite to induce a lactate rise and that the dip and surge might be mechanistically independent from each other. It is important to note that without cellular activity neither lactate dip nor surge occurred, strongly suggesting a cell depolarization-dependent lactate release mechanism[51,52]. Resolving the molecular mechanisms of these respective signalling modalities will require further studies using a combination of specific pharmacological agents and advanced genetic tools.

Arousal strongly induced cortical circuit activation as revealed by EEG and neuronal calcium recordings (Extended Data Figs. 3 and 4), in line with findings from other studies[17,29,36,46]. Neuronal stimulation was recently suggested to trigger neuronal lactate release[11]. However, arousal-induced neuronal activation did not have a neuronal lactate dip that corresponded with an extracellular lactate rise. On the contrary, neurons mainly showed increased lactate levels after the initial astrocytic lactate release (Figs. 1 and 2). In fact, the neuronal lactate increase coincided with a significant slowing of the extracellular lactate rise (threefold decrease), suggesting that the neuronal lactate rise is driven by lactate uptake (Fig. 2). Although neuronal activity may also stimulate glycolysis in neurons[11], it seems unlikely that neurons contain sufficient lactate for it to be released instantaneously (Extended Data Fig. 9). On the one hand, astrocytes have a higher basal glycolytic activity[55] as well as higher in vivo intracellular lactate levels than neurons[10] (Extended Data Fig. 9). On the other hand, astrocytes maintain an intracellular lactate pool (Extended Data Fig. 9c), a phenomenon also observed in astrocytes in vitro even at low lactate levels[51,52]. Thus, lactate release from this 'pressure reservoir' in astrocytes could be rapidly triggered for export in an activity-dependent manner[56].

The arousal-evoked lactate dip in astrocytes was directly followed by a lactate overshoot. This is most likely the reason why more cells were detected showing a dip in vitro[52], whereas more cells showed lactate surges in vivo (Extended Data Fig. 5). This is best explained by having a fast lactate production (aerobic glycolysis) surpassing lactate release covering the initial dip response in vivo. The extracellular lactate elevation period parallels the astrocytic and neuronal lactate surges, suggesting that an increased lactate production is strongly linked to lactate release and uptake, respectively (Fig. 5). Many activity-dependent neuronal signals have been shown to trigger lactate production by glycogenolysis and glycolysis in astrocytes. Astrocytic glycolysis has been seen to be promoted by glutamate, ammonium, nitric oxide and K^+ (refs. [8,51,57,58]) and glycogen breakdown is stimulated by vasoactive intestinal peptide, adenosine, noradrenaline and K^+ (refs. [20,59]). However, in response to arousal, the primary signal responsible for the astrocytic lactate production may well be noradrenaline, as we discuss below.

During arousal, noradrenaline is released throughout the brain from locus coeruleus projections[60]. Noradrenergic signalling has been implicated in cognition and memory formation, particularly that involving β-adrenergic receptors[61–63]. A recent study highlighted that β_2-adrenergic signalling in astrocytes is critical for emotionally driven memory consolidation in mice[15]. Blocking β-adrenergic signalling either pharmacologically with propranolol or by short-hairpin-RNA-mediated knockdown in astrocytes, but not in neurons, impaired formation of long-term memories, which was rescued by administering extracellular lactate[15,16].

We hypothesized that if β-adrenergic signalling is required to mobilize lactate in astrocytes, then we would see a perturbation of arousal-evoked cortical lactate dynamics with pharmacological inhibition. Indeed, 1–6 h after a single intraperitoneal (i.p.) injection of propranolol (10 mg per kg (body weight)), lactate surges in both astrocytes and neurons were strongly reduced (Fig. 3). Notably, the astrocytic lactate dip was not overtly perturbed, indicating that β-adrenergic signalling may not be necessary to facilitate lactate channel opening and/or transporter activity. In fact, astrocytes and neurons remained responsive to arousal-induced cortical activation, as calcium transients were not diminished by blocking β-adrenergic receptors (Extended Data Fig. 6). This is in line with arousal-mediated astrocytic calcium transients being primarily mediated by α-adrenergic but not β-adrenergic receptors[17,46]. Hence, other activity-dependent mechanisms could stimulate the lactate-release machinery in astrocytes, very likely mediated by an acute extracellular $[K^+]$ rise[51,52]. High $[K^+]$ may also participate in the delayed increase in astrocytic lactate, through NBCe1-mediated stimulation of glycolysis[52,64,65] and glycogen degradation[59], acting in concert with the slower stimulation of astrocytic glycolysis by glutamate[8,64].

Inhibition of β-adrenergic signalling via a single i.p. propranolol injection (10 mg per kg (body weight)) reduced arousal-evoked lactate surges in astrocytes by about 35% around 6 h post injection (Fig. 3). It could well be that β-adrenergic receptors were not fully inhibited by a single i.p. injection, and that a higher or prolonged dose, or a locally administered dose, might have had an even stronger impact on glycogen or glucose metabolism, as previously suggested[15,66]. As discussed above, other activity-dependent mechanisms are also likely to be involved in promoting lactate production, such as K^+-mediated acceleration of glycolysis and glycogenolysis[59,64]. It is important to note that while both astrocytes and neurons remained similarly responsive to arousal, indicating that workload and energy demand were unchanged during propranolol treatment, the subsequent reductions in arousal-evoked lactate surges in neurons and astrocytes were primarily caused by a partial deficit in lactate production. Thus, we assume that reductions in arousal-evoked lactate elevations in neurons are directly linked to a reduced lactate mobilization presumably from glycogen stores in astrocytes (Figs. 3 and 5). However, astrocytic β-adrenergic signalling may affect glucose metabolism[19,67,68]. Nonetheless, it is most interesting that a minimal perturbation of β-adrenergic signalling has such a strong impact on cortical lactate dynamics.

Noradrenaline-mediated glycogen breakdown and lactate release[20] were reported to be important for long-term memory formation[3,12]. To obtain a more direct evidence for a functional role of glycogen, we used a mouse model lacking brain-specific GYS1 (Fig. 4 and Extended Data Fig. 8) to study the functional consequences of an absent glycogen store[14]. We found that mice lacking brain glycogen have deficits in associative learning compared with littermate controls (Extended Data Fig. 10c–e). These results are consistent with previous reports showing that glycogen in the brain is critical in learning and memory processes[12,14,15]. GYS1 KO mice, compared with control littermates, revealed neither differences in baseline cellular activity nor differences in blood plasma metabolites, making it unlikely that systemic changes affected the behavioural performance (Extended Data Fig. 8). Importantly, GYS1 KO mice and littermates were similarly responsive to arousal. Hence, the subsequent reductions in arousal-evoked lactate surges in neurons and astrocytes are primarily caused by the absence of glycogen stores (Fig. 4). Since glycogen is predominantly stored in astrocytes, astrocytic β-adrenergic signalling possibly mobilizes lactate from glycogen and explains the arousal-evoked cortical lactate surges. Although direct effects of β-adrenergic signalling on lactate production in cortical neurons cannot be ruled out, it is more likely that astrocytes are critically involved in arousal-evoked lactate mobilization and that lactate derived from glycogenolysis promotes associative learning and long-term-memory formation[12,16] with a common lactate-dependent mechanism that is mediated by β-adrenergic signalling in astrocytes[15].

Astrocytic networks are rapidly activated upon arousal in mice[17,46–48]. Also, astrocytes have been recently described to be critically involved in regulating startle-induced behaviours in *Drosophila* larvae[69]. It is well-known that sensory processing and behavioural responses are strongly influenced by brain-state transitions and periods of increased arousal. Extracellular lactate elevations have been demonstrated to modulate neuronal excitability[21,22], to regulate neuronal signalling and expression of plasticity-related genes[16] and to play an important role in stress- or arousal-induced memory formation[12,15,16]. Our study demonstrates in awake behaving mice that astrocytes rapidly release lactate in response to a startle-induced increase in arousal. In addition, we demonstrate that mice deficient of brain glycogen show reduced arousal-evoked lactate surges and deficits in associative learning behaviour. It is therefore intriguing to speculate that astrocytes release lactate upon arousal not only to fuel neurons but also to modulate neuronal network activity, which may contribute to brain-state-dependent network-signal processing. Future analysis of mice in which lactate channels are selectively removed from astrocytes will help to address the functional impact of startle-induced arousal, fast astrocytic lactate release in the modulation of neuronal network activity and animal behaviour.

In summary, our data favour an activity-induced astrocyte-to-neuron lactate shuttle. We provide in vivo evidence showing that arousal triggers lactate release from astrocytes, and that astrocytic lactate mobilization is partly mediated by β-adrenergic signalling and lactate mobilization from glycogen stores (Fig. 5). Our study opens an exciting avenue for future studies to investigate the contribution of astrocytic lactate release in, for example, brain-state-dependent sensory processing and in higher-order brain functions, such as attention and decision-making.

Methods

Animals. All experimental and surgical procedures were approved by the local veterinary authorities according to the guidelines of the Swiss Animal Protection Law, Veterinary Office, Canton Zurich (Act of Animal Protection, 16 December 2005, and Animal Protection Ordinance, 23 April 2008). Female C57BL/6J

(Charles River) and GYS1 KO[14] mice weighing between 20 and 30 g were used in this study. For control experiments, littermates were used. All mice were kept in standardized single cages with food and water ad libitum. During experimental periods, mice were subjected to water deprivation. Body weight was monitored before and after all training and experimental sessions. If body-weight loss exceeded 15% with respect to the baseline weight, animals would be given free access to water until their weight had normalized. All housed animals were subjected to a 12 h–12 h light–dark cycle with the dark phase adjusted so that the animals were in their active phase during experimental periods. Surgical interventions were performed at age 10–15 weeks. Mean life span of mice for awake experiments was 439.6 ± 166.1 d.

Surgical interventions. Surgical interventions were performed on two separate days. On the first day, the animals were anaesthetized with isoflurane 1.5–2.0% in a mixture of O_2 and air (30%/70%) at a flow rate of 400 ml per min. Vitamin A ointment was applied to avoid corneal desiccation. To prevent dehydration, 0.2 ml of saline solution was subcutaneously injected every hour. Animals were fixed in a stereotaxic frame (Model 900; David Kopf Instruments) for the head-post implantation as previously described by others[70]. In short, fur from the head and neck area was removed, and after disinfection (Kodan; Schülke & Mayr), a 2-cm-long midline incision was made between the eyes, extending to the neck. A bonding agent (Gluma Comfort; Heraeus Kulzer) was applied after cleaning the skull and carefully separating the temporal muscle. Next, a head-cap was formed, made of multiple layers of light-curing dental cement (Synergy D6 Flow; Coltene AG). Finally, a custom-made aluminium head-post was attached, and open skin was attached to the implant with acrylic glue (Histoacryl; Braun). On the second day, a craniotomy was performed using a dental drill (OSSEODOC; Bien-Air), above the left somatosensory cortex, for intracortical virus injection. Animals were anaesthetized with a mixture of fentanyl (0.05 mg per kg (body weight); Sintenyl; Sintetica), midazolam (5 mg per kg (body weight); Dormicum; Roche) and medetomidine (0.5 mg per kg (body weight); Domitor; Orion Pharma) injected i.p., and anaesthesia was maintained with midazolam after 50 min (5 mg per kg (body weight); subcutaneous). A face mask that delivered oxygen was installed to prevent hypoxemia. For multiviral injections in the somatosensory cortex, neighbouring adeno-associated viral (AAV) injections (50–75 nl each) were delivered with a custom-made micro injector as described elsewhere[10] to achieve multiple nonoverlapping loci in the somatosensory cortex. The neuronal construct included a human synapsin-1 (hSYN) promoter and the astrocyte-specific construct included a minimal GFAP promoter (gfaABC$_1$D). Transduction was performed by injecting: a lactate sensor, Laconic[25], (1) for neurons (AAV6-hSYN-Laconic; titre 1.02 E13 VG per ml) and (2) for astrocytes (AAV9-GFAP-Laconic; titre 3.1 E12 VG per ml); and calcium sensors (3) RCaMP 1.07[27] for neurons (AAV6-hSYN-RCaMP 1.07; titre 2.4 E13 VG per ml) and (4) GCaMP6s[26] for astrocytes (AAV9-GFAP-GCaMP6s; titre 3.2 E13 VG per ml) expression, diluted 5–30 times in physiological saline. Injections were performed via a glass capillary to a cortical depth of 300 µm through the intact dura. Large blood vessels were avoided to prevent bleeding and the absorption of light by haemoglobin during imaging. For later chronic optical measurements, a square sapphire glass (3 × 3 mm; Powatec) was gently placed on the dura mater and sealed with light-curing dental cement (Synergy D6 Flow; Coltene AG).

Fluorescence check. Three weeks after injection, the animals were checked for sensor expression. Animals were anaesthetized with 1.5% isoflurane as described above. Excitation light was delivered at 510 nm for an overview of the vessel structure, 490 nm for the excitation of Laconic and GCaMP6s and 600 nm for the excitation of RCaMP by a monochromatic-based illumination system (Polychrome V; Till Photonics). Fluorescence was collected with a fluorescence stereo microscope (Leica MZ16FA with a Plan Apo ×1.0 objective; Meyer Instruments). Vessel images were recorded with a high-performance digital CCD camera system (Pixelfly; PCO) with an exposure time of 50 ms for the vessel images and 500 ms for fluorescence images. We used emission filters for yellow and green (F47-535; AHF Analysentechnik) and for red (F47-623; AHF Analysentechnik) to detect fluorescence emission. Image acquisition was controlled by Camware software (V3.09; PCO). Vessels imagines and fluorescent maps were combined to determine the location of the expression site in respect to the vessel structure.

Behavioural test set-up. A custom-made head-fixation box was built for chronic imaging and constant positioning of the animal. The response-suppression task used in this study was designed to suppress movement for 8-s periods while images from the cortex were acquired. After 8 s, a tone was sounded to indicate the end of each period (reward stimulus). As a reward stimulus, a 70-dB click noise of 1 ms duration with 2–18-kHz bandwidth was produced (background noise was 50 dB) and delivered by stereo speakers positioned 20 cm away from the animal's head. A drinking spout that included a piezo sensor (LDT0-028K; Measurement Specialties) was mounted in front of the animal. The spout was connected to a solenoid valve (Type 0330; Burkert) that controlled water delivery upon spout deflection. A custom-made piezo movement sensor for monitoring movement was positioned under the animal's body. A camera (191133; Conrad Electronic AG) with an infrared light source (BL0106-15-28; Kingbright Electronics) was used for monitoring animals. We used the custom-written LabVIEW program (Version 2012; National Instruments) and multifunctional data acquisition cards to control and monitor all components of the behavioural apparatus[71].

Behavioural paradigm, training and performance. Animals were first handled and familiarized with the experimenter, 1 week after implantation for at least 3 times a day. They were adapted to water deprivation 12 h before training sessions and accustomed to tolerate head fixation and to drink water from a spout every 2 s during training sessions. Finally, the animals were trained in 2 daily sessions not to move for up to 8 s until the reward stimulus was presented. Occurrence of movement during this period led to a temporal delay of the reward stimulus. Delay was computed depending on the time point and the duration of movement within the normal movement-suppression window. After the sound of each tone, the animal was given a 1.5-s-long 'window of opportunity' to lick the spout. After the reward stimulus was triggered by a spout deflection (stimulus response), there was a water release of 0.002 ml of water per trial (referred to as 'reward on lick'). All licks were registered. Licks within the suppression window were counted as false licks. Detected licks within the window of opportunity were counted as correct trials. We computed the number of correct trials for each training session to evaluate performance and training progress of all animals. Only mice that reached a 75% correct trial performance during training were included for awake imaging. On average, mice performed 139 ± 33 trials per session, and 2,835 ± 1,320 total trials.

Isoflurane experiments. In the first set of experiments, we collected data from a 10-min baseline (50 trials) in which the animal was performing the behavioural paradigm, followed by isoflurane administration for 20 min (1.5% isoflurane in O_2 and air (1:2), and 400 ml per min total flow rate) and a recovery phase after turning isoflurane off, for 30 min. In the second set of experiments a baseline of 5 min was acquired followed by administration of isoflurane for 20 s (1.5%) and a recovery phase of 14 min and 40 s (termed ISO pulse).

Different arousal paradigms. For dose-response comparison the ISO pulse protocol was adapted such that either no isoflurane and just air (air pulse) or only 0.75% of isoflurane was supplied through the ventilation mask for 20 s. The isoflurane-pulse paradigm was also used for the administration of amyl acetate. Instead of isoflurane amyl acetate mixed with air (1:1,000; W504009; Merck) was supplied through a ventilation mask for 20 s. For whisker stimulations, whiskers were inserted into a glass capillary (GB120F-8P; 1.5 × 1.05 × 30 mm; Science Products) glued onto the piezo actuator. The whisker stimulus consisted of single-whisker deflections (90 Hz, 8 s) generated by a piezo actuator (T223-H4CL-303X; Piezo Systems). Driving voltage was generated by a custom-written LabVIEW program (National Instruments) using a multifunctional data-acquisition card (PCI-6259; National Instruments) and amplified with a piezo controller (MDT693A; Thorlabs). In all animals, the right γ-whisker was stimulated. For the stimulation of the right whisker pad, a Toohey Spritzer (Toohey Company) was used to deliver air puffs at 5 Hz for 3 s. Driving voltage was generated by an MC stimulus (STG4001; Multi Channel Systems).

Microscope design and imaging parameters. A custom-made two-photon laser scanning microscope[72] equipped with a two-photon laser with <120-fs temporal pulse width (InSight DeepSee Dual; Spectra-Physics) with a ×20 water immersion objective (W Plan-Apochromat ×20/1.0 DIC VIS-IR; Zeiss) was used for image acquisition. Excitation and emission beam paths were separated by a dichroic mirror (F73-825; AHF Analysentechnik). A dichroic mirror at 506 nm (F38-506; AHF Analysentechnik) and 560 nm (F38-560; AHF Analysentechnik) separated the emission light beam. The emission light was focused on the photomultiplier (H9305-03, Hamamatsu) by two lenses (LA1050-A1 and AL5040-A2; Thorlabs). We used emission filters for blue (F39-477; AHF Analysentechnik), green and yellow (F37-545; AHF Analysentechnik) and red (F39-608; AHF Analysentechnik) for multicolour imaging. ScanImage[73] and custom-written LabVIEW software (Version 2012; National Instruments) were used for image control and data acquisition.

Lactate imaging parameters. Anatomical imaging was performed at a resolution of 512 × 512 pixels at a frequency of 0.74 Hz. Emission signals were acquired at 5.94 Hz and with a 256 × 256-pixel resolution. ScanImage[73] and custom-written LabVIEW software (version 2012; National Instruments) were used for image control and data acquisition. Laconic was excited with 870 nm with an overall mean power of 45.8 ± 12.6 mW for neurons and 42.0 ± 12.7 mW for astrocytes. Neurons recorded 131.5 ± 27.1 µm and astrocytes 117.7 ± 25.2 µm below cortical surface. Power measurements were made close to the focal plane of the objective with a thermal power sensor (S370C; Thorlabs) and a digital optical power meter (PM120; Thorlabs).

Lactate analysis. For numerical integrations of the AUC, the MATLAB trapz function was used. Data processing and analysis were carried out with MATLAB 2018a (MathWorks) and ImageJ[74]. Ratiometric data were analysed with the MATLAB toolbox Cellular and Hemodynamic Image Processing Suite CHIPS[37].

Regions of interest (ROIs) were manually selected in ImageJ using high resolution 512 × 512-pixel images.

Calcium imaging parameters. Data were acquired from the somatosensory cortex 100–200 µm below the cortical surface. Anatomical imaging was performed at a resolution of 512 × 512 pixels at a frequency of 0.74 Hz. Emission signals were acquired at 11.84 Hz and with a 128 × 256-pixel resolution. GCaMP6s and RCaMP 1.07 were excited simultaneously with a 940 nm and a power of 57.9 ± 8.1 mW at an imaging depth of 116.6 ± 26.0 µm. Power measurements were made close to the focal plane of the objective with a thermal power sensor (S370C; Thorlabs) and a digital optical power meter (PM120; Thorlabs).

Calcium analysis. Data processing and analysis was carried out with MATLAB 2018a (MathWorks) and ImageJ[74]. Calcium data were analysed with the MATLAB toolbox Cellular and Hemodynamic Image Processing Suite CHIPS[37] as previously described by Stobart et al.[38]. In more detail, all calcium data were spectrally unmixed to reduce potential bleed through of GCaMP6s or RCaMP 1.07 and aligned using a 2D convolution engine to account for motion and x–y drift in time. Background noise was defined as the bottom first percentile pixel value in each frame and was subtracted from every pixel. Regions of interest (ROIs) were selected a by customized implementation of an activity-based algorithm for the automated identification of active neurons or astrocytes (FLIKA in CHIPS). In the activity-based algorithm, a two-dimensional (2D) spatial Gaussian filter (S_{xy} = 2 mm) and a temporal moving average filter (width = 0.1 s RCaMP 1.07 and 0.5 s for GCaMP6s) were applied to all images to reduce noise. Active pixels were identified as those that exceeded a moving threshold (mean pixel intensity plus 7 × s.d. for RCaMP 1.07 and 5 × s.d. for GCaM6s) and had a peak within a defined time window (0.0845–2 s for RCaMP 1.07 and 0.1689–8 s for GCaMP6s) compared with the preceding 5 s. Active pixels were grouped within space (minimum area of 3.78 mm^2 for RCaMP 1.07 and GCaMP6s) and time (0.169 s for RCaMP 1.07 and 1.35 s for GCaMP6s). The 3D mask of active pixels was summed along the temporal dimension, normalized and thresholded (q = 0.33 for RCaMP 1.07 and q = 0.2 for GCaMP6s) to make a 2D activity ROI mask for each channel. Raw image data from pixels within each 2D ROI were statistically compared with pixels surrounding the ROI ($P < 0.05$ by one-way analysis of variance (ANOVA)) to exclude false positives.

EEG, EMG and ECS recordings. EEG, EMG and extracellular glucose and lactate measurements were performed with a commercially available recording system (four-channel EEG/EMG/BIO Tethered System; Pinnacle Technology). All mice had a head-post mounted as previously described, and ROIs were spared from dental cement. Two to five days after the head-post was mounted, the skull was opened with a dental drill. Two EEG screws were implanted bilaterally in the frontal area and two screws (8403; Pinnacle Technology) in the occipital area, and a guide cannula (7032; Pinnacle Technology) was implanted into the primary somatosensory cortex, wired with a head mount (8402; Pinnacle Technology) and fixed with dental cement. Two EMG electrodes were placed in the neck muscle of the animal. After a recovery period of 2 weeks, the precalibrated lactate biosensor (7004; Pinnacle Technology) was inserted into the guide cannula. Prior to implantation, each lactate biosensor was calibrated in vitro to ensure selectivity and sensitivity for lactate. Data were acquired at 250 Hz for EEG and 1 Hz for lactate measurements. Experimental means were used for time-series comparison.

Pupillometry. For recordings of the right pupil, we used a Raspberry Pi NoIR Camera Module V2 night-vision camera, an infrared light source (BL0106-15-28; Kingbright Electronics) and a Raspberry Pi 3 Model B (Raspberry Pi Foundation). Ambient light was mimicked with an ultraviolet-light source (NSPU510CS; Nichia Corporation) confined to the left eye to reduce interference with cortical imaging. Pupil diameter was measured using a custom-written MATLAB (MathWorks) script. Frames were binarized and an ellipse-fitting algorithm (Ellipse Fit; MATLAB; MathWorks) was used to approximate the pupil size.

Blood plasma metabolite measurements. The tail vein was used to measure blood plasma metabolite levels. A blood drop was collected with a test strip used for instant whole-blood glucose (Contour; Bayer) and lactate measurements (Lactate Pro 2; Arkray).

Drug application and imaging protocol. Propranolol, a β-adrenergic receptor antagonist, in saline, was injected i.p. at a concentration of 10 mg per kg (body weight). For control experiments, only saline was injected. The ISO pulse protocol was used for five sequential imaging sessions at 1, 3, 6 and 24 h after the initial recording at 0 h.

Trans-acceleration with pyruvate. For intravenous interventions injections, a 30-G needle was connected to fine bore polyethylene tubing (0.28 mm ID; 0.61 mm OD; Portex; Smith Medical), filled with 0.9% saline solution and inserted into one of the tail veins. The tubing was connected via an X connector (model SC25; Instech) to peristaltic pumps (Reglo digital ISM 831; Ismatec SA) operated with custom-written MATLAB (MathWorks) code. A 500 mM solution of sodium chloride (S7653; Sigma Aldrich) or sodium pyruvate (P2256; Sigma Aldrich) at 4 mM per kg (body weight) was injected for 3 min.

Immunohistochemistry. Mice were anaesthetized with pentobarbital and transcardially perfused directly with 4% PFA in PBS, pH 7.4. Brains were dissected and post fixed in 4% PFA in PBS for 3 h. Tissue was cryoprotected in 30% sucrose in PBS, overnight at 4 °C. Coronal sections (40 µm) were cut using a microtome (KS34; Hyrax) and then stored in antifreeze at −20 °C until further usage. Free floating sections were washed in Tris–Triton (0.05% Triton-X; pH 7.4). For antigen retrieval, slices were put in sodium citrate buffer (10 mM; 0.05% tween20; pH 6) in a water bath in a commercially available microwave, twice for 7 min at 40% of full microwave power. Sections were cooled downs and preincubated in Tris–Triton containing 5% donkey serum and 0.3% Triton-X for 1 h at RT. Primary antibodies were dissolved in preincubation solution, and slices were incubated overnight at 4 °C. After washing in Tris–Triton, secondary antibodies were applied in Tris–Triton for 45 min at RT. Slices were washed in Tris–Triton, mounted on glass slides and covered with Dako Fluorescence Mounting Medium (Code S3023). Primary mouse anti-glutamine synthetase (610518BD; Transduction Lab) (1:500) and rabbit anti-GYS1 (3886S; Cell Signaling) (1:300) antibodies were used. Alexa Fluor488-AffiniPure donkey anti-mouse IgG (H+L) (715-545-151; LucernaChem) (1:700), Cy3-conjugated AffiniPure donkey anti-rabbit IgG (H+L) (711-165-152; LucernaChem) (1:700) were used as secondary antibodies. Images were taken with a Zeiss LSM 700 confocal microscope using a ×40 oil immersion objective (Zeiss). Data were normalized to the mean of all control measurements. A two-tailed unpaired t-test was used for statistical comparison.

Western blot. GYS1-protein deletion in brain-specific GYS1-knockout mice (GYS1 KO) was quantified from cortical protein extracts. Samples were prepared with sucrose buffer (320 mM sucrose; 10 mM Tris (pH 7.4); 1 mM $NaHCO_3$; 1 mM $MgCl_2$) with protease inhibitors (Roche) and bullet blender (Next Advance) with a 1:1 beads to sample volume ratio. The tissue was homogenized by mixing twice for 15 s on setting 4. After centrifugation for 3 min at 14,000 r.p.m., the protein content in the supernatant was determined with the BCA Protein Assay Kit according to the micro scale assay protocol. For the western blot, 25 µg of protein lysate was used per sample and run in a 12% polyacrylamide separating gel, and blotting was performed according to the manufacturer's instructions (Abcam). Membranes were blocked with TBST (0.1% Tween; pH 7.4) containing 5% BSA for 60 min at 4 °C. Primary antibodies were used at the following dilutions: GYS1; 1:1,000 (rabbit; 3886; Cell Signaling Technology); and actin, 1:20,000 (rabbit; A2066; Sigma). These were incubated overnight in the blocking solution. Membranes were washed with TBST (pH 7.4) and incubated with an infrared fluorescence secondary antibody system (LI-COR; Odyssey imagers). The secondary antibody (anti rabbit; 800 nm; LI-COR) was dissolved in TBST containing 1% BSA at a dilution of 1:10,000 and then incubated for 1 h at room temperature before washing in TBST and in TBS. The fluorescent signal was detected by an Odyssey scanner (LI-COR).

Statistics. Statistical analyses and calculations were performed in R (version 3.6.1) using the lme4 package for linear mixed-effects models and multivariate analysis. All data were reported and plotted as uncorrected means and s.d. P values for different parameter comparisons were obtained using the lsmeans or multcomp packages with Tukey's post hoc tests. Also, paired and unpaired t-test was used where appropriate. $P < 0.05$ was considered significant. For data cross-correlation, corrplot from MATLAB's econometrics toolbox was used, with a Pearson's linear correlation coefficient at a significance level of 0.05. The MATLAB ploterr function was used to compute data distribution histogram of correlated data. Estimates of effect sizes (Cohen's d) were calculated using the R package pwr.

Reporting summary. Further information on research design is available in the Nature Research Reporting Summary linked to this article.

Data availability

All data that support the findings of this study are available from the corresponding author upon request. Source Data for Extended Data Fig. 8 are available online.

Code availability

All code that was used in this study is available from the corresponding author upon request. The CHIPS toolbox for MATLAB is freely available on GitHub (https://ein-lab.github.io/)[37].

Received: 8 September 2018; Accepted: 15 January 2020;
Published online: 17 February 2020

References

1. Kety, S. S. & Schmidt, C. F. The nitrous oxide method for the quantitative determination of cerebral blood flow in man: theory, procedure and normal values. *J. Clin. Invest.* **27**, 476–483 (1948).

2. Hu, Y. & Wilson, G. S. A temporary local energy pool coupled to neuronal activity: fluctuations of extracellular lactate levels in rat brain monitored with rapid-response enzyme-based sensor. *J. Neurochem.* **69**, 1484–1490 (1997).
3. Newman, L. A., Korol, D. L. & Gold, P. E. Lactate produced by glycogenolysis in astrocytes regulates memory processing. *PLoS ONE* **6**, e28427 (2011).
4. Yellen, G. Fueling thought: management of glycolysis and oxidative phosphorylation in neuronal metabolism. *J. Cell Biol.* **217**, 2235–2246 (2018).
5. Magistretti, P. J. & Allaman, I. Lactate in the brain: from metabolic end-product to signalling molecule. *Nat. Rev. Neurosci.* **19**, 235–249 (2018).
6. Dienel, G. A. Lack of appropriate stoichiometry: strong evidence against an energetically important astrocyte-neuron lactate shuttle in brain. *J. Neurosci. Res.* **95**, 2103–2125 (2017).
7. Barros, L. F. & Weber, B. CrossTalk proposal: an important astrocyte-to-neuron lactate shuttle couples neuronal activity to glucose utilisation in the brain. *J. Physiol.* **596**, 347–350 (2018).
8. Pellerin, L. & Magistretti, P. J. Glutamate uptake into astrocytes stimulates aerobic glycolysis: a mechanism coupling neuronal activity to glucose utilization. *Proc. Natl Acad. Sci. USA* **91**, 10625–10629 (1994).
9. Wyss, M. T., Jolivet, R., Buck, A., Magistretti, P. J. & Weber, B. In vivo evidence for lactate as a neuronal energy source. *J. Neurosci.* **31**, 7477–7485 (2011).
10. Machler, P. et al. In vivo evidence for a lactate gradient from astrocytes to neurons. *Cell Metab.* **23**, 94–102 (2016).
11. Diaz-Garcia, C. M. et al. Neuronal stimulation triggers neuronal glycolysis and not lactate uptake. *Cell Metab.* **26**, 361–374 e364 (2017).
12. Suzuki, A. et al. Astrocyte-neuron lactate transport is required for long-term memory formation. *Cell* **144**, 810–823 (2011).
13. Zhang, Y. et al. Inhibition of lactate transport erases drug memory and prevents drug relapse. *Biol. Psychiatry* **79**, 928–939 (2016).
14. Duran, J., Saez, I., Gruart, A., Guinovart, J. J. & Delgado-Garcia, J. M. Impairment in long-term memory formation and learning-dependent synaptic plasticity in mice lacking glycogen synthase in the brain. *J. Cereb. Blood Flow Metab.* **33**, 550–556 (2013).
15. Gao, V. et al. Astrocytic β2-adrenergic receptors mediate hippocampal long-term memory consolidation. *Proc. Natl Acad. Sci. USA* **113**, 8526–8531 (2016).
16. Descalzi, G., Gao, V., Steinman, M. Q., Suzuki, A. & Alberini, C. M. Lactate from astrocytes fuels learning-induced mRNA translation in excitatory and inhibitory neurons. *Commun. Biol.* **2**, 247 (2019).
17. Paukert, M. et al. Norepinephrine controls astroglial responsiveness to local circuit activity. *Neuron* **82**, 1263–1270 (2014).
18. Alberini, C. M., Cruz, E., Descalzi, G., Bessieres, B. & Gao, V. Astrocyte glycogen and lactate: new insights into learning and memory mechanisms. *Glia* **66**, 1244–1262 (2018).
19. Dienel, G. A. & Cruz, N. F. Aerobic glycolysis during brain activation: adrenergic regulation and influence of norepinephrine on astrocytic metabolism. *J. Neurochem.* **138**, 14–52 (2016).
20. Sorg, O. & Magistretti, P. J. Characterization of the glycogenolysis elicited by vasoactive intestinal peptide, noradrenaline and adenosine in primary cultures of mouse cerebral cortical astrocytes. *Brain Res.* **563**, 227–233 (1991).
21. Sada, N., Lee, S., Katsu, T., Otsuki, T. & Inoue, T. Epilepsy treatment. Targeting LDH enzymes with a stiripentol analog to treat epilepsy. *Science* **347**, 1362–1367 (2015).
22. Clasadonte, J., Scemes, E., Wang, Z., Boison, D. & Haydon, P. G. Connexin 43-mediated astroglial metabolic networks contribute to the regulation of the sleep-wake cycle. *Neuron* **95**, 1365–1380 (2017).
23. Tang, F. et al. Lactate-mediated glia-neuronal signalling in the mammalian brain. *Nat. Commun.* **5**, 3284 (2014).
24. Morland, C. et al. The lactate receptor, G-protein-coupled receptor 81/hydroxycarboxylic acid receptor 1: expression and action in brain. *JJ. Neurosci. Res.* **93**, 1045–1055 (2015).
25. San Martin, A. et al. A genetically encoded FRET lactate sensor and its use to detect the Warburg effect in single cancer cells. *PLoS ONE* **8**, e57712 (2013).
26. Chen, T. W. et al. Ultrasensitive fluorescent proteins for imaging neuronal activity. *Nature* **499**, 295–300 (2013).
27. Ohkura, M., Sasaki, T., Kobayashi, C., Ikegaya, Y. & Nakai, J. An improved genetically encoded red fluorescent Ca^{2+} indicator for detecting optically evoked action potentials. *PLoS ONE* **7**, e39933 (2012).
28. Franks, N. P. General anaesthesia: from molecular targets to neuronal pathways of sleep and arousal. *Nat. Rev. Neurosci.* **9**, 370–386 (2008).
29. Liu, X. et al. Arousal transitions in sleep, wakefulness, and anesthesia are characterized by an orderly sequence of cortical events. *NeuroImage* **116**, 222–231 (2015).
30. Kum, J. E., Han, H. B. & Choi, J. H. Pupil size in relation to cortical states during isoflurane anesthesia. *Exp. Neurobiol.* **25**, 86–92 (2016).
31. Guedel, A. E. *Inhalation Anesthesia; A Fundamental Guide* (Macmillan, 1951).
32. Chen, C. R. et al. Roles of adrenergic alpha1 and dopamine D1 and D2 receptors in the mediation of the desynchronization effects of modafinil in a mouse EEG synchronization model. *PLoS ONE* **8**, e76102 (2013).
33. McCormick, D. A. & Bal, T. Sleep and arousal: thalamocortical mechanisms. *Annu. Rev. Neurosci.* **20**, 185–215 (1997).
34. Jameson, L. C. & Sloan, T. B. Using EEG to monitor anesthesia drug effects during surgery. *J. Clin. Monit. Comput.* **20**, 445–472 (2006).
35. MacIver, M. B. & Bland, B. H. Chaos analysis of EEG during isoflurane-induced loss of righting in rats. *Front. Syst. Neurosci.* **8**, 203 (2014).
36. Reimer, J. et al. Pupil fluctuations track fast switching of cortical states during quiet wakefulness. *Neuron* **84**, 355–362 (2014).
37. Barrett, M. J. P., Ferrari, K. D., Stobart, J. L., Holub, M. & Weber, B. CHIPS: an extensible toolbox for cellular and hemodynamic two-photon image analysis. *Neuroinformatics* **16**, 145–147 (2018).
38. Stobart, J. L. et al. Cortical circuit activity evokes rapid astrocyte calcium signals on a similar timescale to neurons. *Neuron* **98**, 726–735 e724 (2018).
39. Gibbs, M. E., Anderson, D. G. & Hertz, L. Inhibition of glycogenolysis in astrocytes interrupts memory consolidation in young chickens. *Glia* **54**, 214–222 (2006).
40. Lee, K., Makino, S., Imagawa, T., Kim, M. & Uehara, M. Effects of adrenergic agonists on glycogenolysis in primary cultures of glycogen body cells and telencephalon astrocytes of the chick. *Poult. Sci.* **80**, 1736–1742 (2001).
41. Duran, J. & Guinovart, J. J. Brain glycogen in health and disease. *Mol. Asp. Med.* **46**, 70–77 (2015).
42. Berridge, C. W. & Foote, S. L. Effects of locus coeruleus activation on electroencephalographic activity in neocortex and hippocampus. *J. Neurosci.* **11**, 3135–3145 (1991).
43. Carter, M. E. et al. Tuning arousal with optogenetic modulation of locus coeruleus neurons. *Nat. Neurosci.* **13**, 1526–1533 (2010).
44. Aston-Jones, G. & Cohen, J. D. An integrative theory of locus coeruleus-norepinephrine function: adaptive gain and optimal performance. *Annu. Rev. Neurosci.* **28**, 403–450 (2005).
45. Berridge, C. W. & Waterhouse, B. D. The locus coeruleus–noradrenergic system: modulation of behavioral state and state-dependent cognitive processes. *Brain Res. Brain Res. Rev.* **42**, 33–84 (2003).
46. Ding, F. et al. α1-Adrenergic receptors mediate coordinated Ca^{2+} signaling of cortical astrocytes in awake, behaving mice. *Cell Calcium* **54**, 387–394 (2013).
47. Srinivasan, R. et al. Ca^{2+} signaling in astrocytes from $Ip3r2^{-/-}$ mice in brain slices and during startle responses in vivo. *Nat. Neurosci.* **18**, 708–717 (2015).
48. Slezak, M. et al. Distinct mechanisms for visual and motor-related astrocyte responses in mouse visual cortex. *Curr. Biol.* **29**, 3120–3127 (2019).
49. Zerbi, V. et al. Rapid reconfiguration of the functional connectome after chemogenetic locus coeruleus activation. *Neuron* **103**, 702–718 (2019).
50. Chaigneau, E., Oheim, M., Audinat, E. & Charpak, S. Two-photon imaging of capillary blood flow in olfactory bulb glomeruli. *Proc. Natl Acad. Sci. USA* **100**, 13081–13086 (2003).
51. Sotelo-Hitschfeld, T. et al. Channel-mediated lactate release by K^+-stimulated astrocytes. *J. Neurosci.* **35**, 4168–4178 (2015).
52. Ruminot, I., Schmalzle, J., Leyton, B., Barros, L. F. & Deitmer, J. W. Tight coupling of astrocyte energy metabolism to synaptic activity revealed by genetically encoded FRET nanosensors in hippocampal tissue. *J. Cereb. Blood Flow Metab.* **39**, 513–523 (2019).
53. Pierre, K. & Pellerin, L. Monocarboxylate transporters in the central nervous system: distribution, regulation and function. *J. Neurochem.* **94**, 1–14 (2005).
54. Karagiannis, A. et al. Hemichannel-mediated release of lactate. *J. Cereb. Blood Flow Metab.* **36**, 1202–1211 (2016).
55. Hung, Y. P., Albeck, J. G., Tantama, M. & Yellen, G. Imaging cytosolic NADH-NAD^+ redox state with a genetically encoded fluorescent biosensor. *Cell Metab.* **14**, 545–554 (2011).
56. Kasparov, S. Are astrocytes the pressure-reservoirs of lactate in the brain? *Cell Metab.* **23**, 1–2 (2016).
57. Lerchundi, R. et al. $NH4^+$ triggers the release of astrocytic lactate via mitochondrial pyruvate shunting. *Proc. Natl Acad. Sci. USA* **112**, 11090–11095 (2015).
58. Bolanos, J. P., Delgado-Esteban, M., Herrero-Mendez, A., Fernandez-Fernandez, S. & Almeida, A. Regulation of glycolysis and pentose-phosphate pathway by nitric oxide: impact on neuronal survival. *Biochim. Biophys. Acta* **1777**, 789–793 (2008).
59. Choi, H. B. et al. Metabolic communication between astrocytes and neurons via bicarbonate-responsive soluble adenylyl cyclase. *Neuron* **75**, 1094–1104 (2012).
60. Schwarz, L. A. & Luo, L. Organization of the locus coeruleus-norepinephrine system. *Curr. Biol.* **25**, R1051–R1056 (2015).
61. Cahill, L., Prins, B., Weber, M. & McGaugh, J. L. β-adrenergic activation and memory for emotional events. *Nature* **371**, 702–704 (1994).
62. Murchison, C. F. et al. A distinct role for norepinephrine in memory retrieval. *Cell* **117**, 131–143 (2004).
63. Sun, H., Mao, Y., Wang, J. & Ma, Y. Effects of β-adrenergic antagonist, propranolol on spatial memory and exploratory behavior in mice. *Neurosci. Lett.* **498**, 133–137 (2011).

64. Bittner, C. X. et al. Fast and reversible stimulation of astrocytic glycolysis by K^+ and a delayed and persistent effect of glutamate. *J. Neurosci.* **31**, 4709–4713 (2011).
65. Ruminot, I. et al. NBCe1 mediates the acute stimulation of astrocytic glycolysis by extracellular K^+. *J. Neurosci.* **31**, 14264–14271 (2011).
66. Savaki, H. E., Kadekaro, M., Jehle, J. & Sokoloff, L. α- and β-adrenoreceptor blockers have opposite effects on energy metabolism of the central auditory system. *Nature* **276**, 521–523 (1978).
67. Catus, S. L., Gibbs, M. E., Sato, M., Summers, R. J. & Hutchinson, D. S. Role of β-adrenoceptors in glucose uptake in astrocytes using β-adrenoceptor knockout mice. *Br. J. Pharmacol.* **162**, 1700–1715 (2011).
68. Dong, J. H. et al. β2-adrenergic receptor and astrocyte glucose metabolism. *J. Mol. Neurosci.* **48**, 456–463 (2012).
69. Ma, Z., Stork, T., Bergles, D. E. & Freeman, M. R. Neuromodulators signal through astrocytes to alter neural circuit activity and behaviour. *Nature* **539**, 428–432 (2016).
70. Mayrhofer, J. M., Haiss, F., Helmchen, F. & Weber, B. Sparse, reliable, and long-term stable representation of periodic whisker deflections in the mouse barrel cortex. *NeuroImage* **115**, 52–63 (2015).
71. Mayrhofer, J. M. et al. Novel two-alternative forced choice paradigm for bilateral vibrotactile whisker frequency discrimination in head-fixed mice and rats. *J. Neurophysiol.* **109**, 273–284 (2013).
72. Mayrhofer, J. M. et al. Design and performance of an ultra-flexible two-photon microscope for in vivo research. *Biomed. Opt. Express* **6**, 4228–4237 (2015).
73. Pologruto, T. A., Sabatini, B. L. & Svoboda, K. ScanImage: flexible software for operating laser scanning microscopes. *Biomed. Eng. Online* **2**, 13 (2003).
74. Schneider, C. A., Rasband, W. S. & Eliceiri, K. W. NIH Image to ImageJ: 25 years of image analysis. *Nat. Methods* **9**, 671–675 (2012).
75. Coggan, J. S. et al. Norepinephrine stimulates glycogenolysis in astrocytes to fuel neurons with lactate. *PLoS Comput. Biol.* **14**, e1006392 (2018).

Acknowledgements

We thank all Weber group laboratory members for support and frequent discussions. We would also like to thank J.-C. Paterna and the Viral Vector Facility of the Neuroscience Center Zurich (ZNZ) for virus production. We further thank J. M. Mayrhofer and W. v. d. Behrens for their initial support in establishing the suppression-response task. A.S.S. received support from a Synapsis Career Fellowship Award and the Cloëtta Foundation, M.T.W. is supported by the Hartmann-Müller Foundation, L.F.B. is funded by the Chilean Government through the Centers of Excellence Basal Financing Program of CONICYT, J.D. and J.J.G. are funded by the Spanish MINECO (BFU2017-82375-R) and the National Institutes of Health (NIH-NINDS) (P01NS097197) and B.W. is supported by the Swiss National Science Foundation (SNF number:31003A_156965).

Author contributions

Conceptualization, M.Z., A.S.S., M.T.W. and B.W.; Methodology, M.Z.; Software, M.Z. and K.D.F.; Formal analysis, M.Z. and A.S.S.; Investigations, M.Z., Z.J.L. and L.H.; Resources: J.L.S., J.D., J.J.G. and L.F.B.; Writing—original draft, M.Z. and A.S.S.; Visualization, M.Z. and A.S.S.; Writing—review and editing, M.Z., A.S.S., M.T.W., L.F.B. and B.W.; Supervision and project administration, M.T.W. and B.W.; Funding acquisition, M.Z., A.S.S., M.T.W. and B.W. All authors discussed the results and contributed to revision of the manuscript.

Competing interests

The authors declare no competing interests.

Additional information

Extended data is available for this paper at https://doi.org/10.1038/s42255-020-0170-4.

Supplementary information is available for this paper at https://doi.org/10.1038/s42255-020-0170-4.

Correspondence and requests for materials should be addressed to B.W.

Peer review information Primary Handling Editor: Elena Bellafante.

Reprints and permissions information is available at www.nature.com/reprints.

Publisher's note Springer Nature remains neutral with regard to jurisdictional claims in published maps and institutional affiliations.

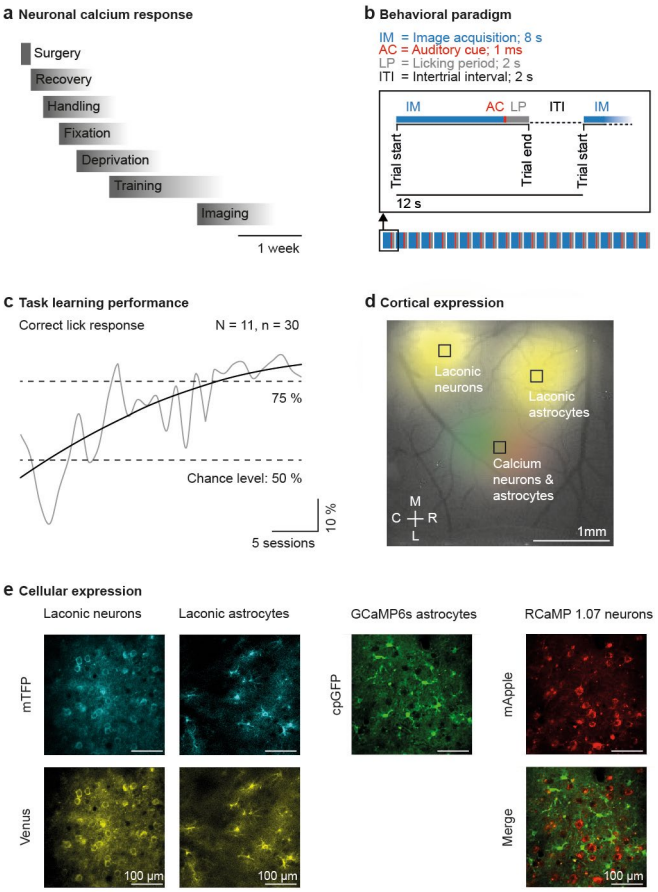

Extended Data Fig. 1 | Awake two-photon imaging to study cortical lactate and calcium dynamics in neurons and astrocytes (Related to Fig. 1). **(a)** Workflow scheme of preparing mice for awake two-photon imaging. Following recovery from surgery and intracortical AAV injections, mice were trained for head-restrained imaging using a suppression-response task and a water reward. On average, mice were ready for imaging at around 4 weeks after surgery. This protocol was repeated for all animals in this study with similar results. **(b)** Behavioral paradigm used during awake imaging. Each trial consisted of an 8 s imaging period (IM) which ended with a 1 ms auditory cue (AC) indicating the mouse to collect the water reward within a lick period of 2 s (LP). Each trial had an intertrial interval (ITI) of 2 s before the next trial started. **(c)** Mean behavioral performance (grey) and learning progress (black) during training. A trial was counted correct when no licking occurred during image acquisition (IM). N = number of animals, n = number of sessions. **(d)** Cortical expression of genetically-encoded lactate sensor Laconic (San Martin et al., [25]), calcium sensor RCaMP 1.07 (Ohkura et al., [27]) and GCaMP6s (Chen et al., [26,32]) imaged through a chronic cranial window. Visualization with single photon excitation. M = medial, L = lateral, C = cranial, R = rostral. **(e)** Representative images of Laconic expression in neurons and astrocytes (mTFP = blue; Venus = yellow), RCaMP 1.07 in neurons (mApple = red) and GCaMP6s in astrocytes (cpGFP = green) and a merge of calcium sensors expressed at the same site (neurons = red, astrocytes = green). Excitation wavelength for Laconic = 870 nm. Wavelength for simultaneous excitation of GCaMP6s and RCaMP 1.07 = 940 nm. Images were taken 121.4 ± 26.9 µm below cortical surface.

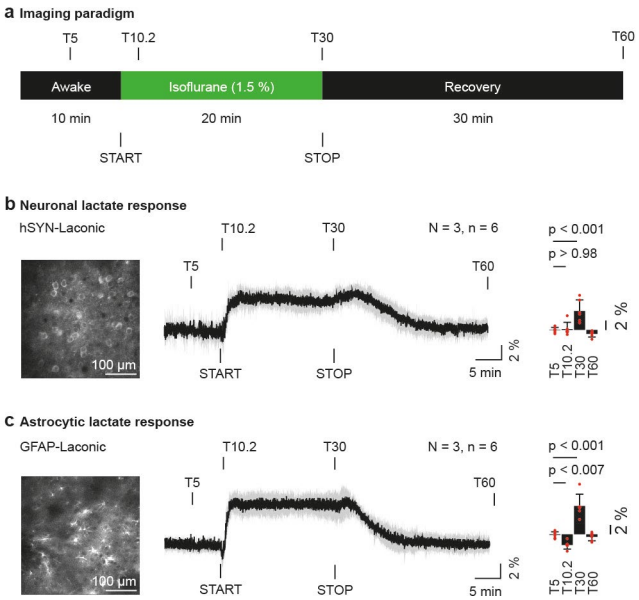

Extended Data Fig. 2 | Lactate dynamics in cortical neurons and astrocytes upon prolonged isoflurane exposure (Related to Fig. 1). (a) Scheme of the prolonged isoflurane imaging protocol. T indicates time points in minutes throughout the imaging session. Time points for the onset (T10) and end (T30) of isoflurane delivery are indicated by START and STOP. **(b, c)** Cortical neurons (b, left panel) and astrocytes expressing Laconic (c, left panel) in individual fields of view. Single cell fluorescence analysis of relative lactate changes (middle panels) during the prolonged isoflurane administration protocol. Both, neurons and astrocytes showed a rise in lactate levels that persisted during the isoflurane period (indicated at T30; relative lactate signal rose by 4.6 ± 1.6% in neurons and 5.5 ± 2.0 % in astrocytes; $p < 0.001$). At T10.2 upon isoflurane induction relative lactate signal dropped by -1.8 ± 1.1 % ($p < 0.007$) in astrocytes only. In contrast, neurons showed no significant lactate decrease when compared to baseline ($p > 0.98$). Lactate levels return to baseline during recovery (indicated at T60). Bar graphs summarize relative changes at T5, T10.2, T30 and T60. Data set contained 104 neurons and 102 astrocytes. T indicates time points in minutes. N = number of animals, n = number of experiments. Data is represented as mean ± SD. m = 6 experiments used to derive statistics. Mean statistics were calculated using two-tailed linear mixed-effects models and Tukey's post hoc tests.

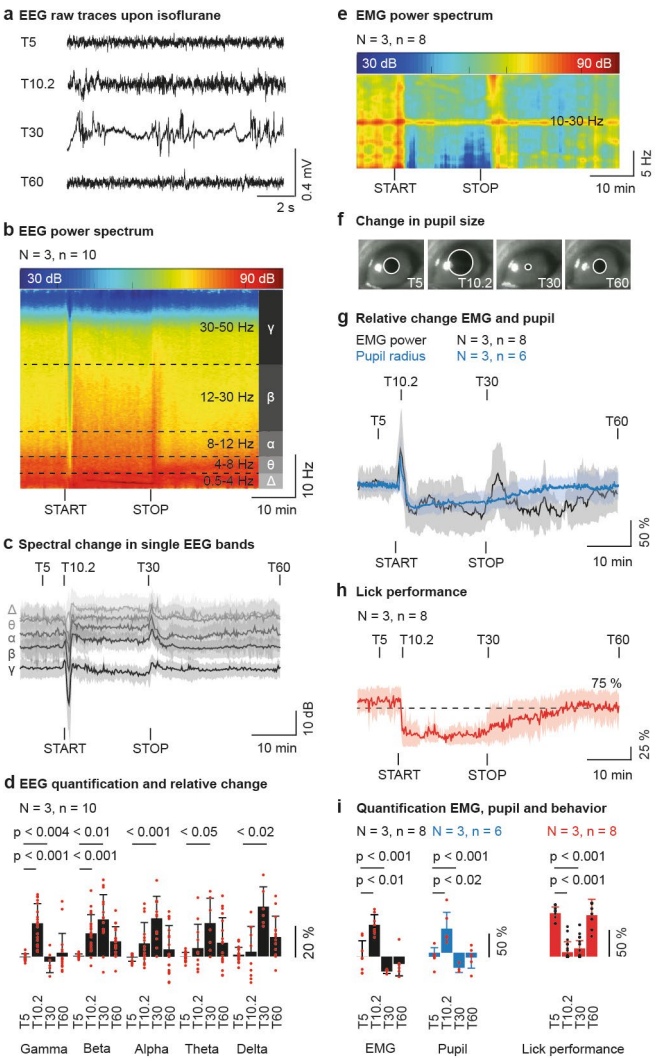

Extended Data Fig. 3 | Isoflurane exposure causes an initial arousal response before reaching the anesthetized state (Related to Fig. 1). (a) EEG raw traces at different time points of the prolonged isoflurane imaging protocol (Extended Data Fig. 2a). Traces represent distinct states such as: T5 = awake behaving, T10.2 = induction and desynchronization, T30 = anesthetized and increased slow-wave activity leading to burst suppression, T60 = recovery and awake. **(b)** EEG power spectrum and EEG bands (delta: 0.5-4 Hz, theta: 4-8 Hz, alpha: 8-12 Hz, beta: 12-30 Hz and gamma: 30-50 Hz) show a clear shift upon isoflurane exposure. Blue = low power (30 dB) and red = high power (90 dB). **(c)** EEG bands according to their power display a biphasic EEG response when transiting from the awake state through the induction phase (increase in high-frequency power) to the anesthetized state (increase in low-frequency power). **(d)** Quantification of EEG bands as a relative change with respect to baseline at time points T5, T10.2, T30 and T60 derived from (c). **(e)** EMG spectrum (10-30 Hz) recorded from neck muscles showed an increase in muscle activity with exposure to isoflurane and a reduced power in the anesthetized state. Blue = low power (30 dB) and red = high power (90 dB). **(f)** Pupillometry analysis revealed pupil dilation in the induction phase (T10.2), then a pupil constriction in the anesthetized state (T30). White circles indicate pupil size approximation. **(g)** Relative changes in EMG power (black) and pupil radius (blue) recorded during the isoflurane protocol. **(h)** Lick performance during the isoflurane protocol. Note that prolonged isoflurane administration immobilized the animal and behavioral performance is absent. **(i)** Quantification of EMG and pupil radius and lick performance at time points T5, T10.2, T30 and T60. Note a significant increase in neuromuscular activity in the induction phase (T10.2) and a reduction in EMG power, pupil size and lick performance during the anesthetized state highlighting that prolonged isoflurane exposure first initiates an aroused state (within the first 60 s), which is then gradually followed by an anesthetized state and immobilization. T indicates time points in minutes. N = number of animals, n = number of experiments. START and STOP indicate the period of isoflurane administration. Data is represented as mean ± SD. m = 10 experiments for EEG, 8 for EMG, 6 for pupil and 8 for lick performance used to derive statistics. Mean statistics were calculated using two-tailed linear mixed-effects models and Tukey's post hoc tests.

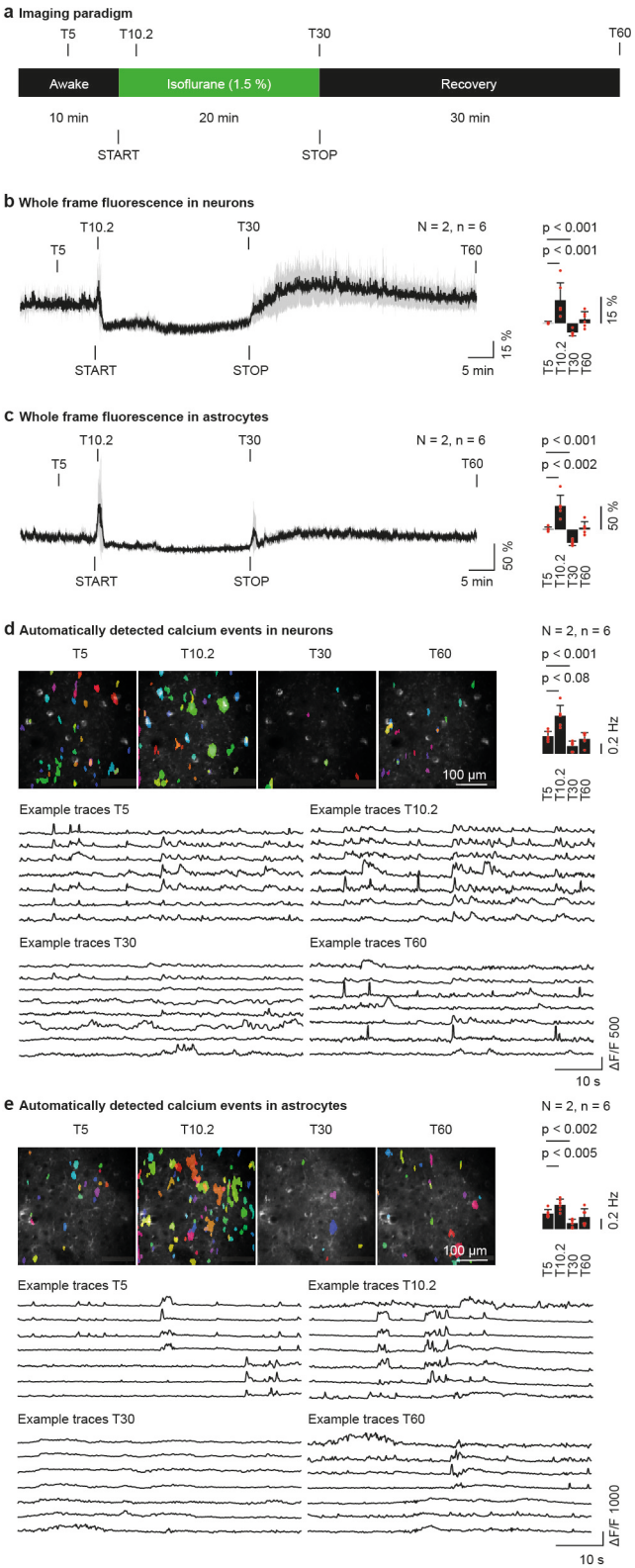

Extended Data Fig. 4 | See next page for caption.

Extended Data Fig. 4 | Calcium activity in neurons and astrocytes upon isoflurane administration (Related to Fig. 1). (**a**) Scheme of the prolonged isoflurane imaging protocol consisting of a 10 min baseline (awake behaving), 20 min isoflurane and a 30 min recovery period. T indicates time in min for the course of the imaging session. Time points for the onset (T10) and end (T30) of isoflurane delivery are indicated by START and STOP. (**b**, **c**) Whole frame fluorescence analysis of relative calcium changes during the isoflurane administration protocol (**a**). The onset of isoflurane exposure (START) caused a strong activation in cortical network and a significant rise in neuronal and astrocytic calcium levels (T10.2). In neurons, whole frame fluorescence intensity increased by 14.2 ± 7.3% ($p < 0.001$) and in astrocytes, it increased by 50.1 ± 21.2 % ($p < 0.001$). During the anesthetized state (T30) overall calcium levels decreased in both cell types and recovered to baseline levels when mice returned to the awake state (T60). Bar graphs on the right summarize calcium level changes at time points T5, T10.2, T30 and T60. (**d**, **e**) Automated analysis to identify calcium events for neurons (**d**) and astrocytes (**e**) using MATLAB toolbox CHIPS (Barrett et al., [37]). Detected signals are indicated by colored ROI masks for time points T5, T10.2, T30 and T60 of the isoflurane administration protocol (**a**). ROIs represent cellular areas of calcium events detected by an automated activity-based algorithm and do not reflect specific manually selected cell structures. Quantification of the number of events detected during these time points are summarized in bar graphs (right). With isoflurane administration there was a significant increase in calcium events in both neurons and astrocytes (T10.2) compared to baseline (T5). Event frequencies were strongly reduced during the anesthetized state (T30) and recovered back to baseline at T60. Example traces illustrate automatically detected events at T5, T10.2, T30 and T60 for neurons (**d**) and astrocytes (**e**). ROI = region of interest. T indicates time points in minutes. N = number of animals, n = number of experiments. Data is represented as mean ± SD. m = 6 experiments used to derive statistics. Mean statistics were calculated using two-tailed linear mixed-effects models and Tukey's post hoc tests.

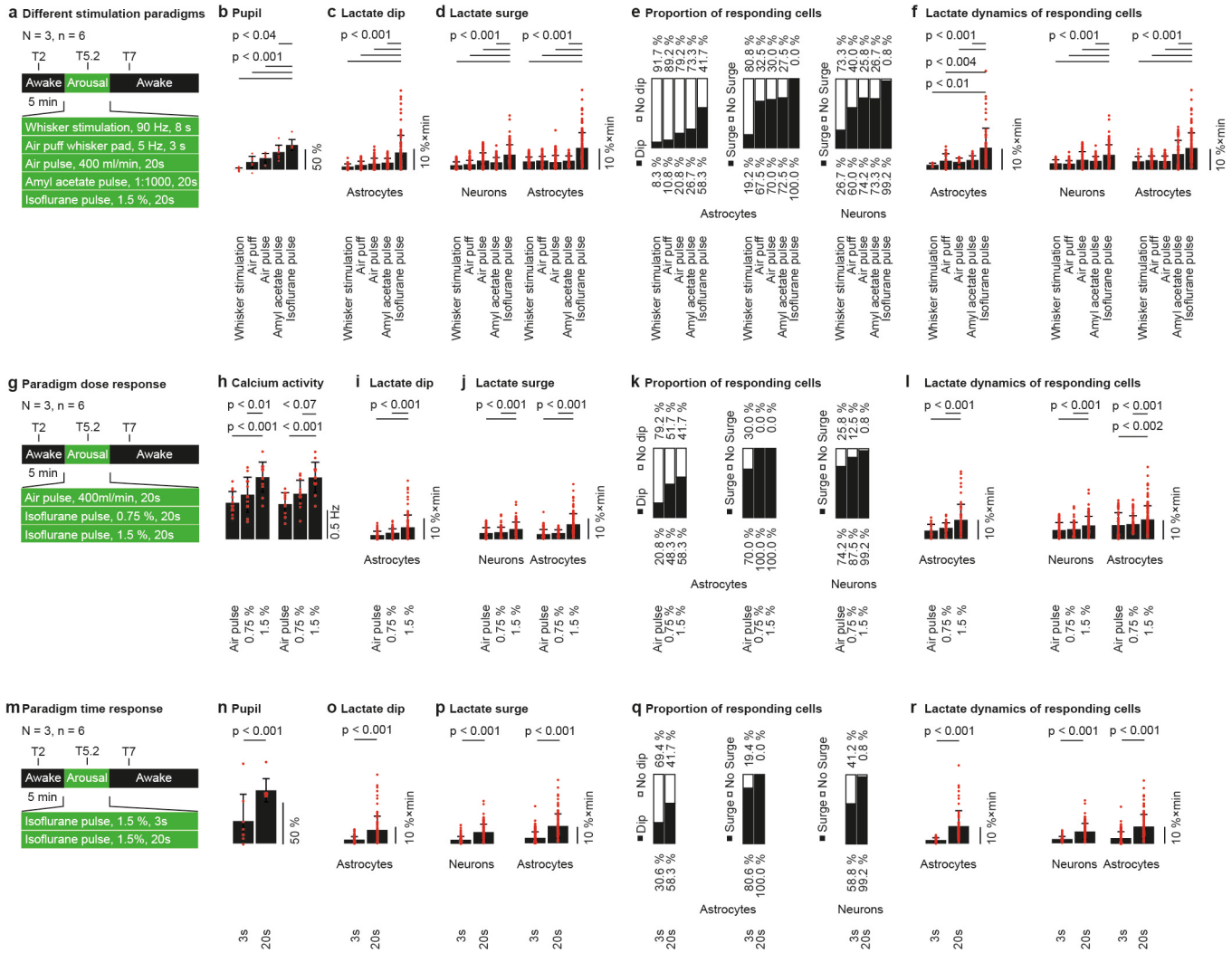

Extended Data Fig. 5 | Comparison of different stimulation paradigms (Related to Fig. 1). (a) Different paradigms to induce arousal in awake mice. **(b)** Comparison of pupil response strengths at T5.2 between the different paradigms. Whisker stimulation induced the smallest response (left) compared to a brief isoflurane pulse (strongest response; right). **(c, d)** Quantification of the area under the curve (AUC) of the stimulation evoked lactate dip in astrocytes (c) and the induced lactate surges in neurons (d; left) and astrocytes (d; right). Note that isoflurane pulse evoked the largest response when compared to other stimulation paradigms. **(e)** Comparison of stimulation paradigms and percentage of responding astrocytes and neurons. Only the ISO pulse mobilized the entire astrocytic and neuronal network. The threshold for a lactate dip (T5.2) or surge (T7) detection was set to 2 SD from baseline values (T2). **(f)** Quantification of lactate dips and surges of only responding neurons and astrocytes identified in (e). **(g)** Dose-dependent stimulation with isoflurane (air pulse, 0.75 % isoflurane and 1.5% isoflurane at 400 ml/min through a ventilation mask). **(h)** Quantification of evoked calcium events in astrocytes and neurons. Note that 1.5% isoflurane evoked the highest number of events. The same field of view was monitored for each paradigm. **(i, j)** The AUC for the dip in astrocytes and the surge in both cell types. **(k)** Percentages of astrocytes and neurons with a lactate response. **(l)** Quantification of the AUC of responding neurons and astrocytes only. **(m)** Time-dependent stimulation with isoflurane. **(n)** Comparison of response strengths measured by pupil response. **(o, p)** Quantification of lactate dips in astrocytes (o), and lactate surges in neurons and astrocytes (p). Note that the 20 s isoflurane pulse evoked a stronger response in neurons and astrocytes when compared to the 3 s stimulation paradigm. **(q)** Comparison of 3 s and 20 s isoflurane pulse stimulation regarding percentages of responding cells. **(r)** Quantification of the AUC of responding neurons and astrocytes only. The threshold for a lactate dip (T5.2) or surge (T7) detection was set to 2 SD from baseline values (T2). The same 120 neurons and 104 astrocytes were monitored for each paradigm. T indicates time points in minutes. N = number of animals, n = number of experiments. Data is represented as mean ± SD. m = 120 neurons and 104 astrocytes for lactate measurements or 6 experiments for calcium and pupil measurements used to derive statistics. Mean statistics were calculated using two-tailed linear mixed-effects models and Tukey's post hoc tests.

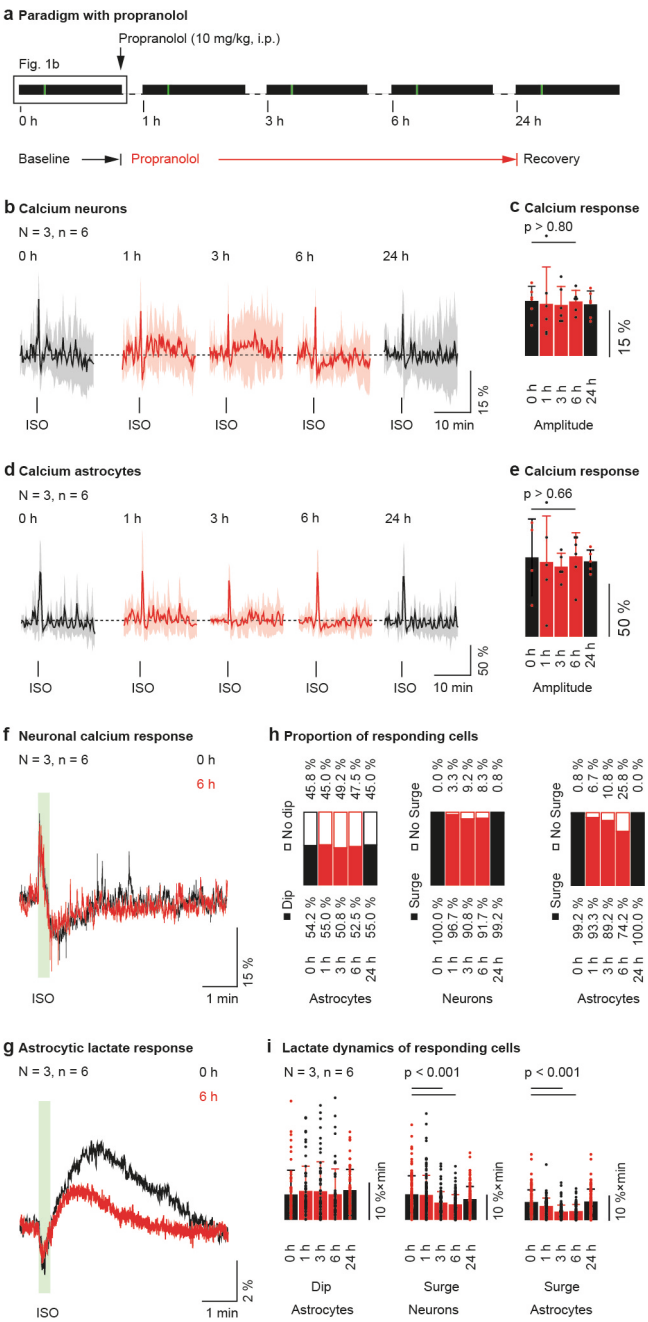

Extended Data Fig. 6 | Propranolol has no effect on cellular calcium activity but reduces lactate surge in astrocytes and neurons (Related to Fig. 3). (**a**) Protocol used to investigate the effects of propranolol in neurons and astrocytes. Propranolol (10mg per kg, i.p.) was injected after baseline acquisition (0 h) and the same cells were imaged in subsequent sessions 1, 3, 6 and 24 h after injection. (**b**–**e**) ISO pulse-evoked calcium changes in neurons (**b**, **c**) and astrocytes (**d**, **e**) at different time points. Signal amplitudes did not differ from control experiments with saline injections (Extended Data Fig. 7). m = 6 experiments used for statistical analysis. (**f**, **g**) Temporal comparison of neuronal calcium and astrocytic lactate response before (0 h; black) and 6 h after (red) propranolol injection. Propranolol had no effect on neuronal calcium response (**f**) and the initial dip in astrocytic lactate upon arousal but it reduced the second phase of lactate mobilization by reducing the astrocytic lactate surge (**g**). Only means are displayed. (**h**) The fraction of astrocytes showing a dip and the fraction of astrocytes and neurons showing an activity-dependent surge. (**i**) The area under the curve (AUC) in responding astrocytes and the AUC of the surge of responding astrocytes and neurons. The threshold for a lactate dip (T5.2) or surge (T7) detection was set to 2 SD from baseline values (T2). The same 113 neurons and 118 were monitored for each paradigm. N = number of animals, n = number of experiments. Data is represented as mean ± SD. m = 113 neurons and 118 astrocytes for lactate measurements used to derive statistics. Mean statistics were calculated using two-tailed linear mixed-effects models and Tukey's post hoc tests.

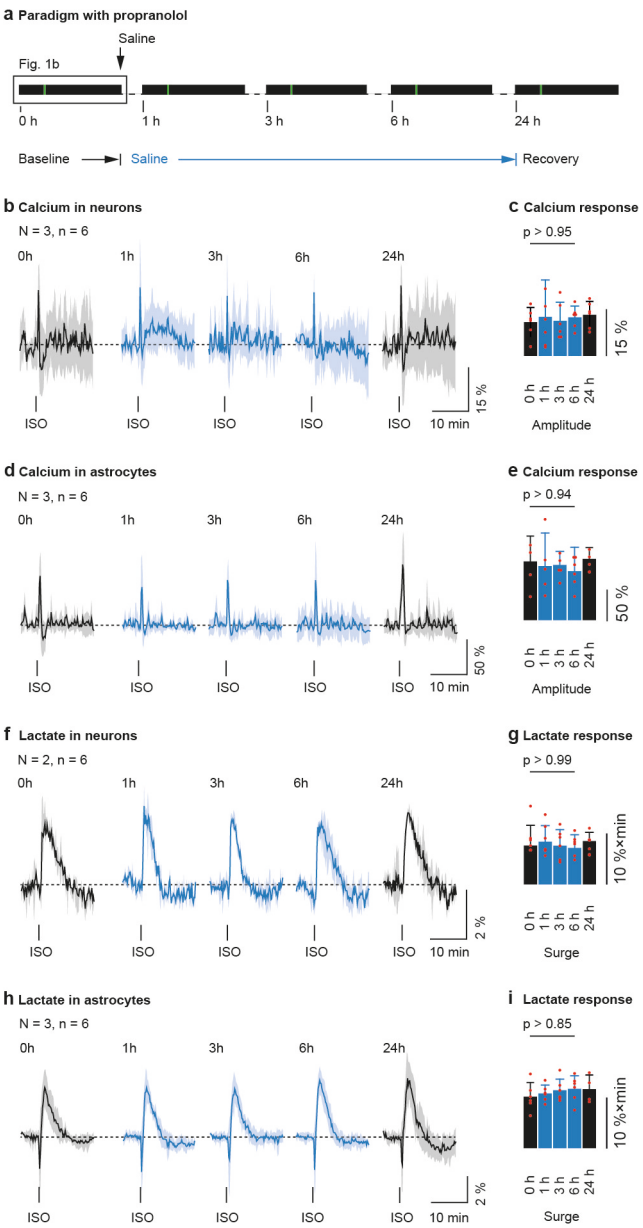

Extended Data Fig. 7 | Control saline experiments of calcium and lactate responses in neurons and astrocytes (Related to Fig. 3). (a) Scheme of the control protocol with saline for arousal-induced calcium and lactate responses in neurons and astrocytes. The same cells as in the propranolol paradigm were monitored in sequential imaging sessions. **(b–e)** Evoked calcium responses in neurons (**b**, **c**) and astrocytes (**d**, **e**). Calcium responses were not affected by saline injection. **(f–i)** Evoked lactate response in neurons (**f**) and astrocytes (**h**) before and after saline injection (0 h - 24 h). The same 113 neurons and 118 astrocytes were monitored in 6 experiments per time point. The isoflurane-induced lactate response in neurons (**g**) and astrocytes (**i**) was not affected by saline injection. Data is represented as mean ± SD. N = number of animals, n = number of experiments. Data was binned into 12 s fragments for data visibility in (b), (d), (f) and (h). m = 6 experiments used to derive statistics. Mean statistics were calculated two-tailed using linear mixed-effects models and Tukey's post hoc tests.

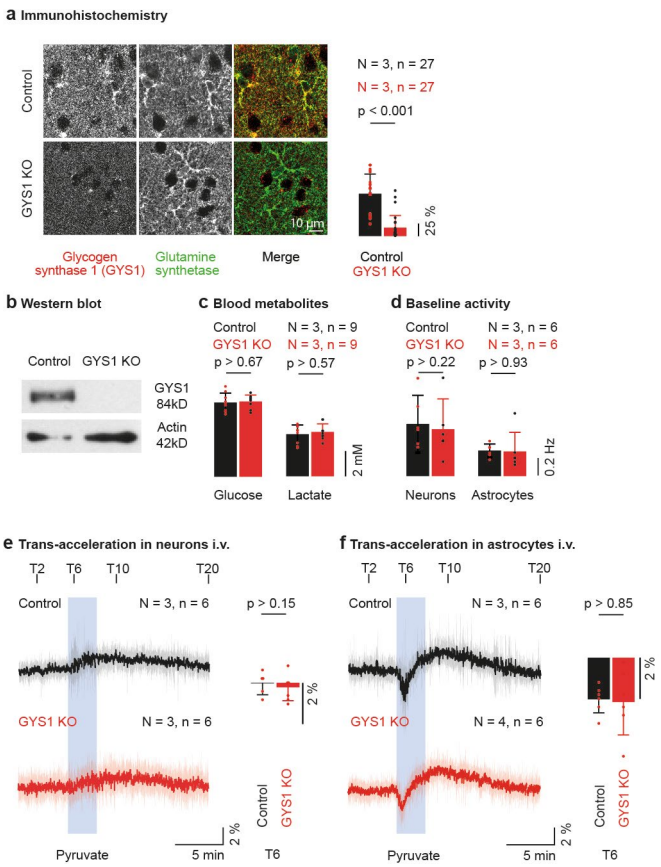

Extended Data Fig. 8 | Comparison of control animals and GYS KO mice (Related to Fig. 4). (a) Immunohistological analysis of GYS1 KO (bottom) and control animals (litter mates; top) of cortical glycogen synthase 1 (GYS1; red) and glutamine synthetase (green). The merge illustrates loss of GYS1 in GYS1 KO mice. Graph represents quantification of the fluorescence intensity of GYS1 (17.2 ± 24.2 %) normalized to the mean of all control animals (100.0 ± 48.2 %; $p < 0.001$). **(b)** Western blot analysis of GYS1 protein abundance in GYS1 KO and control cortical tissue. Actin was used as loading control. Experiment was repeated 3 times with similar results. **(c)** Blood plasma glucose (left panel) and lactate (right panel) did not differ between GYS1 KO and control animals. **(d)** Automatically detected calcium events in cortical neurons (left) and astrocytes (right) in GYS1 KO mice (red) and littermate control animals (black). Both have a similar resting state activity. **(e, f)** One-point calibration with trans-acceleration (3 min; 500 mM pyruvate; i.v.) did not differ between GYS1 KO and control mice. Data set for control animals comprised 110 neurons and 102 astrocytes. Data set for knock-out animals comprised 108 neurons and 87 astrocytes. N = number of animals, n = number of experiments. Data is represented as mean ± SD. m = number of experiments as stated in the representing figure used to derive statistics. Mean statistics were calculated using two-tailed linear mixed-effects models and Tukey's post hoc tests.

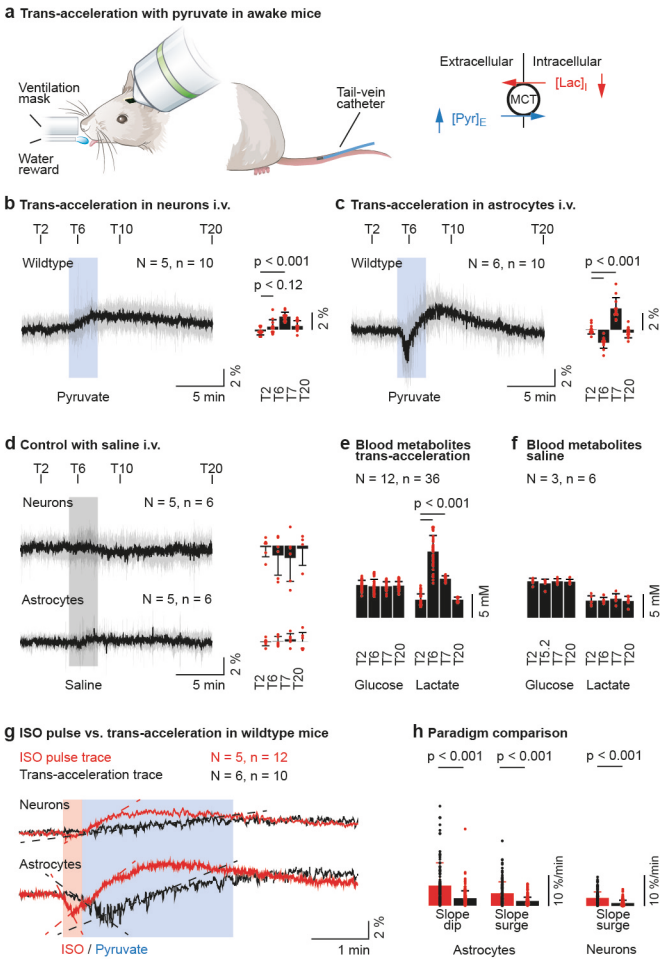

Extended Data Fig. 9 | Comparison of lactate levels in neurons and astrocytes (Related to Fig. 4). (a) Trans-acceleration with pyruvate through a tail-vein catheter for one-point calibration of relative intracellular lactate levels in neurons and astrocytes in awake mice. A bolus injection of pyruvate (3 min; 500 mM; i.v.) artificially increased blood pyruvate levels that entered the brain through monocarboxylate transporters (MCT). Sudden increase in extracellular pyruvate (blue; top right) led to a rapid extrusion and decrease in intracellular lactate (red; top right). This process is termed trans-acceleration. MCT = monocarboxylate transporter. **(b, c)** A bolus injection of pyruvate resulted in a significant decrease in astrocytic (**c**) but not neuronal lactate levels (**b**) indicating significantly higher lactate levels in astrocytes. **(d)** Saline bolus injections had no effect on intracellular lactate levels. For trans-acceleration and saline experiments, the same cells were imaged. m = 6 experiments used for statistical analysis. **(e)** Trans-acceleration increased blood plasma lactate levels (**e**; right panel) leading to an overshoot of lactate in neurons and astrocytes (**b**, **c**). Glucose plasma levels remained stable (**e**; left panel). **(f)** Saline had neither an effect on blood plasma glucose nor lactate levels. **(g, h)** Comparison of the temporal kinetics of the ISO pulse (red) and trans-acceleration (black) protocol illustrating significant differences in kinetics. N = number of animals, n = number of experiments. Data is represented as mean ± SD. For the comparison 226 neurons and 236 astrocytes for the ISO pulse, and 230 neurons and 200 astrocytes for the trans-acceleration paradigm were used to derive statistics. Mean statistics were calculated using two-tailed linear mixed-effects models and Tukey's post hoc tests.

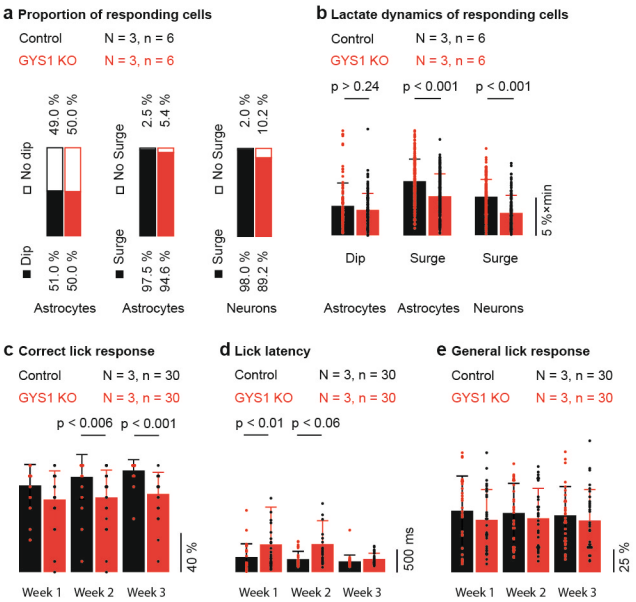

Extended Data Fig. 10 | Loss of brain glycogen leads to impaired lactate surges and associative learning in GYS1 KO mice (Related to Fig. 4). **(a)** Comparison of responsive cells of control (black) and GYS1 KO mice (red). **(b)** Quantification of the area under the curve (AUC) of responding neurons and astrocytes for the dip and surge identified in a. Astrocytes and neurons with a surge had a lower AUC in GYS1 KO animals. For statistical analysis 177 neurons and 146 astrocytes were used. **(c)** GYS1 KO mice (red) showed impaired learning performance in the suppression-response task when compared to control animals (black) resulting in more errors per trial. **(d, e)** Both groups reduced the response latency to the auditory cue, however, GYS1 KO mice responded significantly slower than the control (**d**) although GYS1 KO were similarly responsive (**e**). N = number of animals, n = number of experiments. Data is represented as mean ± SD. m = 30 sessions used to derive statistics. Mean statistics were calculated using two-tailed linear mixed-effects models and Tukey's post hoc tests.

nature research

Corresponding author(s): Bruno Weber

Last updated by author(s): Nov 13, 2019

Reporting Summary

Nature Research wishes to improve the reproducibility of the work that we publish. This form provides structure for consistency and transparency in reporting. For further information on Nature Research policies, see Authors & Referees and the Editorial Policy Checklist.

Statistics

For all statistical analyses, confirm that the following items are present in the figure legend, table legend, main text, or Methods section.

n/a	Confirmed
☐	☒ The exact sample size (*n*) for each experimental group/condition, given as a discrete number and unit of measurement
☐	☒ A statement on whether measurements were taken from distinct samples or whether the same sample was measured repeatedly
☐	☒ The statistical test(s) used AND whether they are one- or two-sided *Only common tests should be described solely by name; describe more complex techniques in the Methods section.*
☐	☒ A description of all covariates tested
☐	☒ A description of any assumptions or corrections, such as tests of normality and adjustment for multiple comparisons
☐	☒ A full description of the statistical parameters including central tendency (e.g. means) or other basic estimates (e.g. regression coefficient) AND variation (e.g. standard deviation) or associated estimates of uncertainty (e.g. confidence intervals)
☐	☒ For null hypothesis testing, the test statistic (e.g. *F*, *t*, *r*) with confidence intervals, effect sizes, degrees of freedom and *P* value noted *Give P values as exact values whenever suitable.*
☒	☐ For Bayesian analysis, information on the choice of priors and Markov chain Monte Carlo settings
☒	☐ For hierarchical and complex designs, identification of the appropriate level for tests and full reporting of outcomes
☒	☐ Estimates of effect sizes (e.g. Cohen's *d*, Pearson's *r*), indicating how they were calculated

Our web collection on statistics for biologists contains articles on many of the points above.

Software and code

Policy information about availability of computer code

Data collection	Scanimage (Reference given in paper, freely available code)
Data analysis	CHIPS (Reference given in paper, freely available code), R, Matlab, Matlab codes are available upon request to the corresponding author.

For manuscripts utilizing custom algorithms or software that are central to the research but not yet described in published literature, software must be made available to editors/reviewers. We strongly encourage code deposition in a community repository (e.g. GitHub). See the Nature Research guidelines for submitting code & software for further information.

Data

Policy information about availability of data

All manuscripts must include a data availability statement. This statement should provide the following information, where applicable:

- Accession codes, unique identifiers, or web links for publicly available datasets
- A list of figures that have associated raw data
- A description of any restrictions on data availability

All data are available from the corresponding author upon request.

Field-specific reporting

Please select the one below that is the best fit for your research. If you are not sure, read the appropriate sections before making your selection.

☒ Life sciences ☐ Behavioural & social sciences ☐ Ecological, evolutionary & environmental sciences

For a reference copy of the document with all sections, see nature.com/documents/nr-reporting-summary-flat.pdf

Life sciences study design

All studies must disclose on these points even when the disclosure is negative.

Sample size	Sample sizes were calculated using the R package pwr.
Data exclusions	Data were excluded in case of strong movements of the animals.
Replication	Data were replicated by using several animals and by repeating the experiments in each animal.
Randomization	Randomization was not performed, as all the animals were treated with all experimental conditions.
Blinding	Blinding was not performed in this study.

Reporting for specific materials, systems and methods

We require information from authors about some types of materials, experimental systems and methods used in many studies. Here, indicate whether each material, system or method listed is relevant to your study. If you are not sure if a list item applies to your research, read the appropriate section before selecting a response.

Materials & experimental systems

n/a	Involved in the study
☒	☐ Antibodies
☒	☐ Eukaryotic cell lines
☒	☐ Palaeontology
☐	☒ Animals and other organisms
☒	☐ Human research participants
☒	☐ Clinical data

Methods

n/a	Involved in the study
☒	☐ ChIP-seq
☒	☐ Flow cytometry
☒	☐ MRI-based neuroimaging

Animals and other organisms

Policy information about studies involving animals; ARRIVE guidelines recommended for reporting animal research

Laboratory animals	C57BL/6J mice (Charles River), GYS1flox/flox mice (Reference given in paper), Nestin-Cre mice (Jax)
Wild animals	*Provide details on animals observed in or captured in the field; report species, sex and age where possible. Describe how animals were caught and transported and what happened to captive animals after the study (if killed, explain why and describe method; if released, say where and when) OR state that the study did not involve wild animals.*
Field-collected samples	*For laboratory work with field-collected samples, describe all relevant parameters such as housing, maintenance, temperature, photoperiod and end-of-experiment protocol OR state that the study did not involve samples collected from the field.*
Ethics oversight	*Identify the organization(s) that approved or provided guidance on the study protocol, OR state that no ethical approval or guidance was required and explain why not.*

Note that full information on the approval of the study protocol must also be provided in the manuscript.